SLAC-PUB-1836
U.C.S.C. 76-053
November 1976
(T/E)

Inelastic Charged-Lepton Scattering off Nucleons*

Clemens A. Heusch
University of California
Santa Cruz, California

Invited Report to the
International Neutrino Conference
Aachen, Germany
June 8-12, 1976

*Work supported in part by the Energy Research and Development Administration

In this review, I am going to present data on the final-state products in deeply inelastic scattering processes of muons and electrons off nucleon targets. Since the nucleon structure functions are being discussed elsewhere in this Conference, I will restrict my report to final-state hadrons, as observed in several recent experiments.

Why have the organizers for the first time included this topic in the agenda of this Neutrino Conference? Maybe it is due to a feeling of collective guilt on the part of the neutrino community - since, ever after the surprising discovery during one of the Aspen Summer Studies for the "200 GeV" accelerator that muons and neutrinos originate jointly in hadron decays, muon experimenters at NAL subjected to the requirements of their neutrino colleagues feel they have suffered from the consequences.

More to the point, neutrino physicists must feel a twinge of envy toward a field where the incoming lepton can be "seen", its charge and momentum defined. The cross-sections for deeply inelastic $(e,\mu)p$ scattering are vastly larger than in the corresponding neutrino case, so that high-statistics studies of detailed features are possible. If we understand the many-channel conspiracy that leads to scaling in ep, μp, that will undoubtedly enhance our knowledge of the corresponding phenomena in νN, $\bar{\nu} N$ scattering. I will therefore concentrate on features that lend themselves to comparisons between e,μ and neutrino scattering.

What features can we usefully study in the process

$$\ell^{\pm} + N \to \text{leptons} + \text{hadrons?} \tag{1}$$

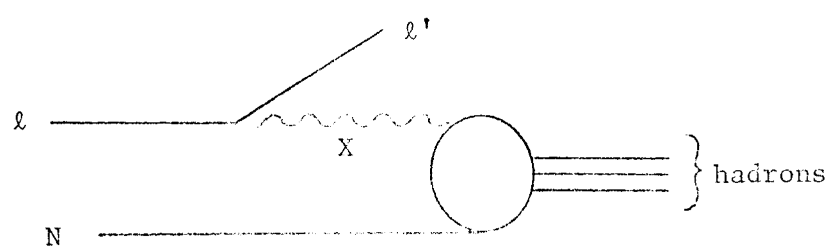

Table I gives beam, exchanged system, and final-state lepton for the reactions we want to compare:

ℓ	ℓ'	X	Remarks on currents
$e^{\pm}$	$e^{\pm}$	γ^{*}	"hadronic component" of variable mass,
$\mu^{\pm}$	$\mu^{\pm}$	γ^{*}	polarization; 2 isospin components.
$\overset{(-)}{\nu}$	$\mu^{\pm}$	$W^{(\pm)}$	V, A currents.
$\overset{(-)}{\nu}$	$\overset{(-)}{\nu}$	Z^{0}	Weak neutral current, current structure not fully established.

It is then clear that the final-state hadrons will provide a probe both for the nucleon's structure and for the structure of the current. This is most easily seen in terms of two particular models for the scattering process:

1) Local current-quark interaction:

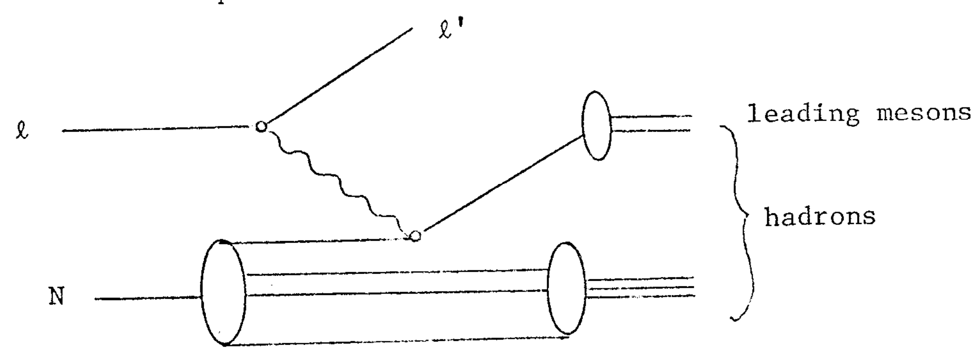

will lead to leading particles telling principally for the quarks/partons into which the nucleon virtually dissociates. In quark-model language, these are the valence constituents.

2) A diffractive picture, on the other hand, exchanges virtually no information other than kinematic between projectile and target. Leading hadrons are therefore telling for the projectile: current fragmentation at its purest.

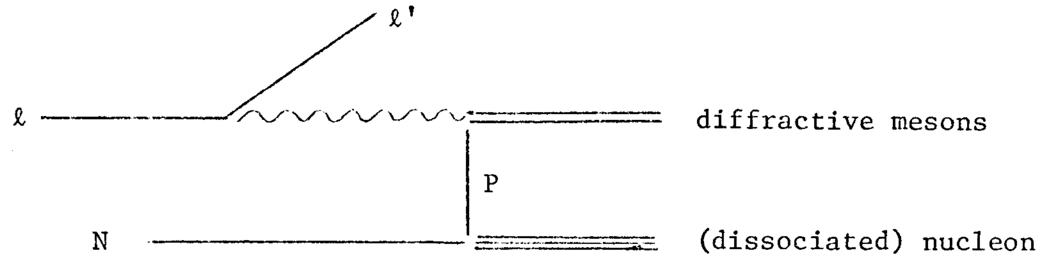

The first of these pictures concentrates on the "bare" virtual photon as the local probe coupling, in a mode assumed to be known, to the individual subconstituent of the target. All properties of leading hadrons can therefore be related to properties of the struck parton each; clearly, we will concentrate on these hadrons.

Caution will be advisable due to the second picture: diffractive diagrams contribute to the leading particle spectrum, but tell us nothing about the struck particle. The parallel to vector-meson photoproduction, wherewe diffract the real photon off a nucleon, becomes important: as we follow a materialization of the electromagnetic current through Q^2 changes, we will want to look for comparable data from neutrino scattering. For parton considerations, we may prefer to attempt the subtraction of clearly diffractive contributions from the data sample.

We will discuss data on the following observables: multiplicities, topologies, leading exchanges, energy and momentum distributions, charge ratios, and discernible diffractive channels. Wherever possible, we will compare with neutrino-induced data.

Experiments

We have three recent experiments with new data, mostly as yet unpublished, on these observables: SLAC experiments 97 (SLAC-MIT) and 72/104 (Santa Cruz/SLAC), and FNAL experiment 98 (Chicago-Havard-Illinois-Oxford).

Tables II gives their relative figures of merit.

Table II

Figures of Merit for Three Experiments

Experiment	SLAC E-97	SLAC E-72, E-104	FNAL Exp. 98
Collaboration	SLAC-MIT	UCSC-SLAC	Chicago-Harvard-Illinois-Oxford
Beam particles, energy (GeV)	e^-, 20.5 GeV	μ^+, 14 GeV	μ^+, 150 GeV
"Cost" of one beam particle	1 e^- at 20.5 GeV	10^9 e^- at 20 GeV	10^7 p at 400 GeV
Integrated beam flux	10^{14}	2.5×10^{10}	2.2×10^{10}
Target material, thickness (cm)	liquid H_2,D_2 4 cm	liquid H_2,D_2 40 cm	liquid H_2 120 cm
Principal detector	forward spectrometer	streamer chamber	forward spectrometer
Acceptance for trigger leptons	$\lvert\vec{p}_{\parallel}\rvert$ > 4 GeV	$\lvert\vec{p}_{\parallel}\rvert$ > 3 GeV	$\lvert\vec{p}_{\parallel}\rvert$ > 15 GeV
for hadron secondaries	$\lvert\vec{p}_{\parallel}\rvert \gtrsim 1.5$ GeV	$\sim 4\pi$	$\lvert\vec{p}_{\parallel}\rvert$ > 8 GeV
# deeply inelastic events	100k in H_2 200k in D_2	10k in H_2 20k in D_2	4,4 k in H_2
# events $Q^2 > 1 (GeV/c)^2$	20k in H_2 40k in D_2	1,6 k in H_2 3,0 k in D_2	3,3 k in H_2
s range (GeV^2)	15 - 31	4 - 25	20 - 250
4-C fits for all-charged final states?	no	yes	no
hadron identification?	yes	no	no
Status of experiment	completed	completed	analysis in progress; more data taking scheduled

Note that these figures apply for the data submitted to this Conference, not for the entire experimental program.

The SLAC-MIT Collaboration concentrates on forward-emitted hadrons to be momentum- and velocity-analyzed by a magnetic spectrometer (Figure 1) containing large proportional wire chambers in conjunction with a large-aperture magnet. A 20 GeV electron beam hits a 4 cm liquid hydrogen (or deuterium) target, emitting hadrons and scattered electrons into a forward acceptance of 230 mr x 400 mrad. The trick of the experiment is the avoidance of radiative backgrounds by means of the arrangement of a superconducting tube in the center of the forward cone, which guides non-interacting beams and small-angle secondaries through a field-free region.

Its particular strength is the separation of charged nucleons, kaons and pions for part of the forward acceptance by use of a threshold Cerenkov counter. The experiment is geared to the observation of the current fragmentation region. Data reported to this Conference are limited to the kinematical range

$$15 \leq s \leq 31 \ (\mathrm{GeV})^2$$

$$0 \leq p_\perp^2 \leq .64 \ (\mathrm{GeV}/c^2)$$

$$.4 \leq z \leq .85 \ ,$$

where z is the fractional energy variable $z \equiv \frac{1}{\nu} E^{\mathrm{lab}}_{\mathrm{hadron}}$.

The Santa Cruz-SLAC set up is shown in Figure 2. An essentially halo-less 14 GeV positive muon beam of great purity is focused in the center of a 40 cm long, 2 cm diameter liquid hydrogen (deuterium) target inside a 2m long streamer chamber. Within the usual limitations of a streamer chamber inside a strong (16 kG) magnetic field, this hadron detector provides almost 4π solid-angle detection of charged secondaries. The triggering counter banks, interleaved with a hadron spoiler, afford between 60 and 90% efficiency for deeply inelastic muon scatters. The advantage of the experiment lies in the full definition of the charged final state, permitting four-constraint fits of such telling channels as $\mu p \to \mu p \rho^o (\rho^o \to \pi^+\pi^-)$, and its relative freedom from radiative effects. Its limitation is in the available center-of-mass energy ($4 \leq s \leq 25$) and Q^2 range ($\lesssim 4.5$).

In contrast to the pair-produced, unpolarized muons produced at SLAC, FNAL Experiment 98 (Figure 3) has a muon beam of well-defined polarization, which illuminates a 120 cm long liquid hydrogen target. The relatively poor angular definition and the vexing halo intensity are partially offset by the installation of multiwire chambers upstream of the target. The forward spectrometer consists of nothing less than the old Chicago cyclotron magnet, permitting momentum analysis of hadrons of $p_{\shortparallel} \gtrsim 8$ GeV/c; scattered muons, momentum-analyzed in the spectrometer, penetrate a number of steel/wire chamber units; for $p_{\shortparallel} \gtrsim 15$ GeV/c, their acceptance is largely assured to trigger a large set of trajectory-defining chambers. The experiment's strength is clearly its kinematic range of $20 \leq s \leq 250$; its weaknesses are its limited momentum acceptance and its severe beam halo difficulties. Data reported here are the results of a first, partial analysis.

From these three experiments, we have a fairly complete set of data on charged hadron production features: multiplicity distributions, energy and momentum distributions, charge ratios, particle ratios, diffractive vector meson production.

As we follow these features through their dependence on such kinematical parameters as energy $W = \sqrt{s}$, fractional longitudinal momentum $x_F = \frac{p_{\shortparallel}}{p_{\shortparallel,max}}$, transverse momentum $p_{\perp}$, and momentum transfer Q^2, an instructive picture emerges. The links to, and differences from, the situation emerging in neutrino-nucleon scattering are particularly telling. Remember, however, that against the large number of events available in electro- or muoproduction (see Table II), for ν and $\bar{\nu}$ charged-current events we have only on the order of 1,000 reported bubble chamber events at this time; for the neutral current events, there are essentially no detailed data yet: neutrino counter experiments cannot at present give data of useful quality for detailed final-state studies.

Charged Hadron Multiplicities

Does overall hadron production depend strongly on the beam particle? Its charge, mass, quantum numbers? Figure 4 shows that the principal trend of hadron multiplicities is with energy, irrespective of the identity of the beam particle. The comparison between photoproduction, electro- (or muo-) production and πp collisions shows only minor differences at small W(or s) values. The photo- and electro- production values lie between π^{+}- and π^{-}- initiated collisions.

What then is the influence of the incoming channel, aside from its determination of $W = \sqrt{s}$? The charged-lepton-induced data put us in the unique position of being able to choose the "mass" Q^2 of our beam particle, the virtual photon. Figure 5 shows $\langle n \rangle$ for different Q^2 values, at fixed W. Clearly, there is no Q^2 trend to the data: the photon "mass" is of no influence. Can we carry this through to time-like photons ($Q^2 = -q^2 < 0$)? In Figure 6, we notice that multiplicities from e^+e^- collisions are consistently above those from μp initiated reactions, for given s. The discrepancy, however, turns out to be a consequence of baryon number conservation: If we plot $\langle n \rangle$ as a function of the energy freely available for particle production, $Q = \sqrt{s} - \Sigma m_{in}$ (upper energy scale of Figure 6), agreement is excellent.

Let us now compare with neutrino scattering: in Figure 4, the νN data are represented by a straight line. It is parallel to, and about one-half unit above the linear fit to the muoproduction data.[1] This is again due to conservation of an incoming charge: the data are due to charged-current (cc) interactions

,


,

which, due to lepton number conservation, mean an added unit of charge for the incoming channel. For $\bar{\nu}$ cc reactions, we therefore expect a parallel trend at some lower level, and first indications are that this may in fact be the case. Why is this different from the case of $\pi^{\pm}$ interactions, with a trend to equal $\langle n \rangle$ values? One obvious difference is the absence of an accessible diffractive channel for neutrino interactions. There are no data available yet on neutral-current ν, $\bar{\nu}$ interactions.

Is there any dependence on the charge of the target nucleon? Figure 7 shows that this is decidedly <u>not</u> the case. The UCSC-SLAC results indicate there is no systematically different energy trend for proton or neutron targets. We will come back to this point in the next section.

<u>Result</u>: charged-hadron multiplicities, once charge conservation laws (Q,B,L,...) have been duly satisfied, depend universally on the energy of the hadronic system. Among the charges, the electric charge Q appears to have minimal effect.

<u>Partial Cross-section</u>

Once we notice that the most prominent trait of the global hadron multiplicity is its lack of specific dependence on the incoming particles' identity, the next question is: how do the - obviously widely different - constituent cross-sections conspire to produce this overall feature? In Figures 8 and 9, we plot, for both proton and neutron targets, the dependence of specific prong cross-sections on energy W and on photon "mass" Q^2. (Note that the hadron prong numbers have to be odd for proton targets, even for the neutron case.)

The energy dependence (Figure 8) is reasonably plausible in terms of constituent cross-sections above the resonance region - notably single π production for one-prong events, diffractive vector meson production, etc. What must appear very astonishing is the Q^2 dependence of the prong cross sections (Figure 9), where in all cases reported the trend is flat, from the lowest Q^2 points measured in muoproduction, $Q^2 \approx 0.2$, up to $Q^2 \approx 4.5$ GeV^2. Add to this surprise the fact that the photoproduction, $Q^2 = 0$, points are very different in the one- and three-prong plots but not in the two-prong sample. We then have a picture of remarkable regularity: the different channels contributing to a given number of hadronic prongs pool their (often widely varying) Q^2-dependences to produce a flat Q^2 behavior out to $Q^2 = 4.5$. Compared to photoproduction, the turn-on of the longitudinal photon component at $Q^2 > 0$ leads to an immediate increase in the one-prong fraction, a decrease in the three-prong fraction: one-pion exchange, which favors the longitudinal photon, often leads to one-prong final states; vector meson production, which is observed to diminish considerably from photo- to electroproduction, (cf. below) is an important part of the three-prong sample. Two-prong events, which show no jump from $Q^2 = 0$ to $Q^2 = 0.2$, appear to even out the one-pion-exchange and the diffractive features.

Result: Marked differences between production from real and virtual photons exist in 1, 3-prong fractions of the total cross-section, and are plausible in terms of the turn-on of the longitudinal cross-section. There is no further dependence on photon "mass" Q^2. Neutrino data, dotted into Figure 8, are too tentative to either corroborate this picture or contradict it.

To further understand the similarity between the overall energy and Q^2 trend of multiplicities from $\gamma^* p$ and $\gamma^* n$, we can break up all of the corresponding prong cross-sections into those that incorporate the dissociation

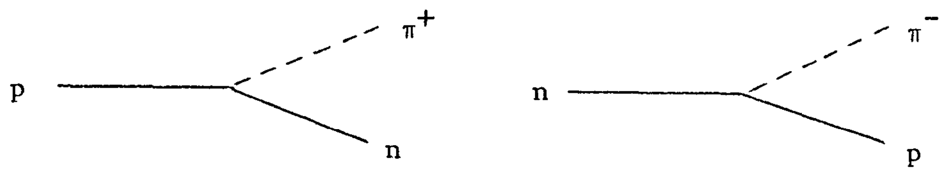

which we will denote "charge exchange" cross sections (CEX), and the "direct" cross-sections, where the nucleon emerges with its initial charge. Note that, for a proton target, they yield the same final multiplicity, whereas for a neutron target, the CEX process increases the multiplicity by two units. In Figure 10, we plot the energy dependence of the quantities

$$\alpha_n = \frac{\sigma_{n,\mathrm{direct}}}{\sigma_{n,\mathrm{direct}} + \sigma_{n,\mathrm{exchange}}} \quad ,$$

and notice that the easiest choice for equal $\langle n\rangle_p$ and $\langle n\rangle_n$, $\alpha_n = \frac{1}{2}$, is by no means realized. Rather, an interpretation in terms of leading exchanges plus the influence of the turn-on of the longitudinal photon appear to make a plausible case for both the energy trend and the Q^2 trend shown in Figure 11.[2]

Energy and Longitudinal Momentum

While the overall multiplicities will, with rising energy, be dominated increasingly by the central kinematical region of small center-of-mass momentum, we expect the specificity of individual reactions to show most clearly in the leading hadrons. Let us see whether we can in this fashion get a glimpse at the underlying dynamics.

As appropriate variables, we choose the fractional laboratory energy

$$z = \frac{1}{\nu}\ E^{\mathrm{had}}_{\mathrm{lab}} \ ,$$

with $\nu = E_\ell - E_{\ell'}$, the virtual photon's laboratory energy; the transverse momentum $p_\perp$ (which we will study in the next section); and the fractional longitudinal momentum in the photon-nucleon center-of-mass system,

$$x_F = \frac{p_{\shortparallel}^*}{p_{\shortparallel\,max}^*} \ , \quad \text{with } p_{\shortparallel\,max}^* \simeq \frac{W^2 - m_p^{\,2}}{2W} \ .$$

This is the Feynman scaling variable, which we denote x_F to avoid confusion with the Bjorken scaling variable

$$x = \frac{1}{\omega} = \frac{Q^2}{2m_p \nu} \ .$$

The distribution of the available energy onto the final-state hadrons is readily described in terms of the structure function

$$F_{\mu p}^{had}(z) = \frac{z}{\sigma}\frac{d\sigma}{dz} \ ,$$

where $\frac{d\sigma}{dz}$ is the inclusive cross-section for the production of hadrons of the type under consideration. Integration over z thus yields the appropriate multiplicity. Figures 12 a,b show these structure functions for negative and positive hadrons, for an s range from 10 to 25, and different bins of the scaling variables $\omega' = 1 + \frac{s}{Q^2}$. While the z trend appears to depend somewhat on ω', the distribution for <u>all</u> hadrons, positive plus negative, is shown in Figure 12c[3] to exhibit a universal trend. As a matter of fact, a comparison with hadrons from e^+e^- collisions[4] follows precisely the same trend. Clearly, these distributions must have a fundamental significance.

Let us, before we figure out what that might be, look at similar structure functions reported by the FNAL collaboration at much higher energies. Fig. 13 gives them in terms of a variable $x' \simeq x_F$, which, for high energies and $x' \gtrsim 0.4$, is essentially coincident with z. Significantly, the values for s>100 not only confirm the lower-energy data of the UCSC/SLAC results, but also find essential similarity between μp and μn data. A comparison with SPEAR data again yields good agreement.

What then is the reason for this common behavior? In terms of a quark-parton model a' la Feynman,[5] the functions $F_{\mu p}$, $F_{e^+e^-}$,... can be built up out of the parton distribution functions $P_i(\omega')$ for the particular case, and the functions $D_i^{\,h}(z)$ which describe the fragmentation of the parton of type i into a hadron h of fractional energy z. In the expression

$$F^h(\omega',z) = \frac{z}{\sigma(\omega')}\frac{d\sigma^h}{dz} = \sum_i z\, P_i(\omega')\, D_i^h(z),$$

we can neglect the presence of strange quark partons (so that we have $i = u, d, \bar{u}, \bar{d}$), and assume that C invariance holds, so that $D_u^+ = D_{\bar{u}}^-$, etc. This leaves us, for the quantities plotted in Fig. 12, with

$$F^+_{\mu p}(\omega',z) = z\,[P_u(\omega')\,D_u^+(z) + (1 - P_u(\omega'))\,D_u^-(z)]$$

$$F^-_{\mu p}(\omega',z) = z\,[P_u(\omega')\,D_u^-(z) + (1 - P_u(\omega'))\,D_u^+(z)]$$

$$F^{+\text{ and }-}_{\mu p}(\omega',z) = z\,[D_u^+(z) + D_u^-(z)].$$

As observed, the structure functions for positives and those for negatives are not only different (as expected from a forward charge ratio $\neq 1$), but depend on ω'; for all hadrons together, however, we find F to be a universal function of z. The similarity of the appropriate $F_{e^+e^-}$ has the interesting implication that the "dressing" of the bare partons into observable hadrons, as described by the fragmentation functions, is the same in the nucleon field

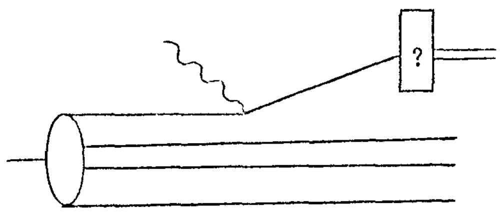

as in the meson-hadronic field <u>in statu nascendi</u>:

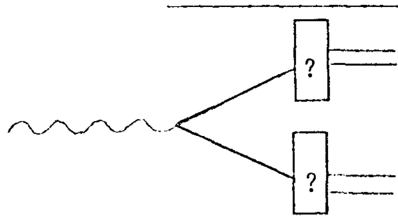

What about the neutrino comparison? For leading negative hadrons, Fig. 14 gives a splendid demonstration(3) that the parton picture with universal fragmentation functions has some merit. Since neutrino interactions exchange a W^+, antineutrino collisions a W^-, the appropriate comparison with our previous assumptions leads to the relations

$$F_{\nu p}^{-} = z\, D_u^{-} ,$$

$$F_{\bar{\nu} p}^{-} = z\, D_u^{+} ;$$

the agreement with the prediction from the μp data is remarkable (after application of a known 15% correction for forward protons).

Transverse Momentum Distributions

We now look at $p_\perp$, where both muon experiments report a flattening of the exponential fits to $d\sigma/dp_\perp^2 \sim e^{-\beta p_\perp^2}$ with increasing x_F (Fig. 15), with the exception of very high x_F particles to be associated with diffractive effects. The mean value of $p_\perp$ plotted vs. x_F (Fig. 16) exhibits, in the range observed, the seagull effect familiar from hadronic interactions.[6] To make sense of the flattening of the $p_\perp$ distributions, let us pick two x_F regions of relatively constant $p_\perp$: $|x_F| < 0.15$ and $0.25 \le x_F \le 0.75$. The $p_\perp$ dependences for these two regions (Fig. 17) display a remarkable two-component behavior:

- → an exponential $e^{-5.3\, p_\perp^2}$ describes both hadron charges for the higher -x_F region;
- → the same exponential provides a good fit to the high -$p_\perp$ part ($p_\perp^2 > 0.3$) of the low -x_F (central rapidity) region:
- → a considerably steeper exponential ($e^{-15 p_\perp^2}$) fits the low -$p_\perp$ part of the central x_F region;
- → the exponentials for positives and negatives differ by a factor of two in normalization, for the higher -x_F region.

Fig. 18 illustrates this two-component behavior further: the mean transverse momentum increases monotonically with W for all except the central region; there, it rises slowly or not at all in the range accessible to the UCSC/SLAC experiment. Preliminary data from FNAL indicate that $p_\perp$ remains constant above $W \stackrel{\sim}{\sim} 5$ GeV, at $\langle p_\perp \rangle \stackrel{\sim}{\sim} .35$, for all x_F combined.

Does $\langle p_\perp \rangle$ depend on the momentum transfer (photon mass-squared) Q^2? Not noticeably (Fig. 19) - a feature that is very much shared by neutrino reactions. This is interesting in terms of a vector-dominance model, where higher-mass states might, for increasing Q^2, be called upon to saturate the hadronic current.

Result: The transverse momentum indicates a two-component behavior. It can be explained either in terms of a universal $p_\perp^2$ slope $\stackrel{\sim}{\sim} 5$, with a steeper slope for second-generation mesons that have to share the parent's $p_\perp$; or of production off valence and sea quarks, respectively.[7] There is no indication of a Q^2 trend of the transverse momentum.

Charge Ratios

The overall hadronic charge ratio is given, in terms of the mean charged multiplicity, by

$$R(\text{all } x_F) = \frac{\langle n \rangle + 1}{\langle n \rangle - 1}$$

which, for $s \to \infty$, increasing $\langle n \rangle$, tends to a value of one. The increase in $\langle n \rangle$ is fed by the central region, where we expect a priori

$$R(x_F \text{ small}) \stackrel{\sim}{\sim} 1,$$

so that any dynamical information on specific interaction features is expected in the higher x_F range (excluding however, the diffractive region, where dissociation of the neutral γ^* would again lead to $R \stackrel{\sim}{\sim} 1$). The simple parton model with fractionally charged quark partons makes very definite predictions on the charge ratio for leading particles (say, $0.4 \le z_F \le 0.8$).[8]

Remember that, in Fig. 18, we noted an almost exact factor of two between the positive and negative $p_\perp^2$ expotentials. Measurements of the ratio R are reported from all three experiments; some are shown in Figs. 20,21.

The Q^2 trend both for all hadrons, and for pions only, is shown from the SLAC/MIT collaboration in Fig. 20, for p and n targets. There appears to be some slight increase up to $Q^2 \simeq 2$, hovering not far from 2 for protons, not far from 1 for neutrons. If the SLAC-MIT claim of a significant excess over unity is accepted for the neutron charge ratio, that could be a result very specific to a fractional-charge quark parton model.[8]

Particle Ratios

From the fragmentation functions determined above under given assumptions, we could in fact have predicted a charge ratio for forward hadrons _if_ we had some knowledge of the parton distribution functions, $P_i(\omega')$, inside the nucleon. Using P_i obtained from inelastic nucleon forum factor data,[9] the UCSC-SLAC collaboration derives a forward charge ratio

$$R = \frac{D_u^{\pi^+}}{D_u^{\pi^-}} \qquad (0.4 \leq z \leq 0.8)$$

of 3.2 ± 0.6 in the absence of any correction for the presence of charged hadrons other than pions. In fact, new data from the SLAC-MIT Group now give us the possibility to correct for the presence of other hadrons.

Fig. 22 gives the ratios of kaons and nucleons to pions, as a function of Q^2. The K^+/π^+ ratio is considerable; all ratios appear to have increased noticeably from their photoproduction values, although it is hard to establish any further Q^2 trend. (Note that elastic ρ^0 events were removed from the data.)

Using these ratios, we can now re-evaluate the charge ratio in the presence of other particles, and wind up with the prediction

$$R\ (0.4 \leq z \leq 0.8) \approx 1.9 \pm 0.4$$

which, in fact, is well matched to the situation observed in Fig. 20.

Current Fragmentation Vector Meson Production

a: ρ^0 production

The vector mesons, ρ^0, ω^0, ϕ^0, sharing the quantum numbers of the photon, have borne the brunt of informing us of the hadronic properties of the real photon via their photoproduction and the link provided by the vector meson dominance model. Can they be similarly employed here, far removed from their poles at $Q^2 = -0.5$ or 1.0, respectively?

Results on ρ^0 production are reported by all three collaborations; on ω^0 by UCSC/SLAC; on ϕ^0, we have only a limit, although the SLAC/MIT data contain relevant information waiting for final analysis.

Clean ρ^0 samples are available from streamer chamber 4-C fits (Fig. 23). ρ^0 samples from the forward spectrometers are less independent of assumptions on shape factors and background subtractions (Fig. 24). However, the diffractive character of ρ^0 production is beautifully demonstrated at FNAL energies (Fig. 25).

A simultaneous fit of the UCSC-SLAC 4C fit sample to the hypothesis

$$\mu^+ p \to \mu^+ p \pi^+ \pi^- ,$$

with $(p\pi^+) = \Delta^{++}$, $(p\pi^-) = \Delta^0$, $(\pi^+\pi^-) = \rho^0$, plus phase space yielded some 250 ρ^0 events, with a cross-section indicated in Fig. 26.

For higher energies, the FNAL forward spectrometer yields, from a total of 184 plausible dipion events almost entirely at $Q^2 < 1$, an extrapolation to $Q^2 = 0$ which can be seen as a first measurement of ρ^0 photoproduction at an energy of $\sim$100 GeV. The resulting values, though with considerable errors, bear out what a simple quark-model-cum - vector-dominance picture would make us expect from the known $\pi^\pm p$ cross-sections (Fig. 27).

What are the points of principal interest in ρ^o production from virtual photons[2]. One persistent question without a convincing answer is whether the Q^2 trend can be described in terms of a vector dominance inspired propagator dependence (for transverse virtual photons)

$$\sigma_\rho(Q^2) \sim \left(1 + \frac{Q^2}{m_\rho^2}\right)^{-2} \times \sigma_\rho(Q^2 = 0)$$

The higher-statistics studies of the SLAC-MIT group confirm the UCSC result(10) that, despite considerable effort,there is no respectable way, at this time, to make the data fit such a dependence, in particular at small Q^2. (Fig. 28). Some claims to the contrary(11) may be founded on the considerable latitude of ρ^o photoproduction cross-sections and their energy dependence as quoted in the literature.

It may therefore be more straightforward to present data in terms of quantities measured in one experiment. Fig. 29 shows, from UCSC/SLAC and SLAC/MIT, fractional ρ^o cross-sections $\sigma_\rho/\sigma_{tot}(Q^2)$, where both numerator and denominator are determined from the same data. The principal feature is the steep fall-off from photoproduction to the lowest measured electroproduction points, and only a gentle decrease with Q^2 beyond that point. I hope the vector dominance experts among our colleagues will give us a plausible argument for this feature shown clearly by the two SLAC experiments.

A second question is to what extent the drop-off of σ_ρ/σ_{tot} between $Q^2 = 0$ and $Q^2 > 0.2$ can account for the sudden decrease of the 3-prong topological cross-section. A drop-off accounting for some 10% of the total cross-section can be explained for the W range $\sim$2.5 - 3. Together with ω production, this goes a long ways toward saturating the change. The flatness above $Q^2 > 0.2$ of σ_3/σ_{tot} is less convincingly mirrored in the ρ^o data: the highest - Q^2 point of SLAC/MIT indicates a possible trend to lower σ_ρ/σ_{tot} values at $Q^2 > 3$.

Lastly: "does the photon shrink"? Ever since the inconclusive results presented by Berkelman at the 1971 Cornell Conference[(12)], the dependence of the slope parameter for the diffractive ρ^{o} forward peak

$$\frac{d\sigma_{\rho}}{dt} \sim a^{\,b(Q^2)\,t}$$

has been an open question. I am afraid that the three sets of data contributed to this Conference do not fully erase this problem: Fig. 30 shows, however, that there is very little if any convincing substance to the long-held belief that $b(Q^2)$ is a monotonically decreasing function.

b: ω,ϕ production

We have some new data on production of the less favored vector mesons: ω mesons through their dominant $\pi^{+}\pi^{-}\pi^{o}$ decay mode, permit one - constraint fitting in the streamer chamber data. Fig. 31 shows that their small width allows convincing background subtraction procedures. Based on some 50 events UCSC/SLAC report a fractional ω cross-section which, above the isobar region, has Q^2 characteristics very similar to ρ^{o} production: a steep fall-off at very small Q^2 values, virtual flatness beyond $Q^2 \gtrsim 0.2$ (cf. Fig. 29). What is most remarkable about this common trend is the $\sigma_{\rho}/\sigma_{\omega}$ ratio, which remains constant within errors from photoproduction through $Q^2 = 3$, although the relative importance on the total cross-section decreases by a factor of at least three (see Fig. 32).

The streamer chamber experiment also reports on a search for 4C fits to the hypothesis $\gamma^{*}p \rightarrow p\,K^{+}K^{-}$; only one plausible candidate for ϕ production and subsequent decay into the $K^{+}K^{-}$ mode survived. Accepting this event for an upper cross-section limit, we determine for the cross-section ratio of ρ, ω, and ϕ mesons over the range $0.2 \leq Q^2 \lesssim 3.5$

$$\sigma_{\rho} \;/\; \sigma_{\omega} \;/\; \sigma_{\phi} \simeq 53 \;/\; 13 \;/\; 1,$$

which is very close to the ratio observed in photoproduction at comparable energies. The SLAC/MIT data are rumored to contain a more respectable ϕ sample; we should soon know whether this remarkable indication holds up.

Result: Good samples of ρ^{o}, ω^{o} events furnish definite evidence that there is a rapid drop-off in relative importance of vector meson production between $Q^2 = 0$ and $Q^2 \approx 0.2$. The ratio of ρ to ω and, possibly, ϕ production is well-remembered by the "increasingly bare" photon. There is no convincing evidence for photon shrinking.

What about comparison data from neutrino physics? This is obviously an extremely fertile field for studies of a meson spectrum that we expect to mirror the structure of a little-understood current. CVC should link the vector part of neutral weak current fragmentation to the data just discussed - but there is not even a hint of data at this time. Fragmentation of the axial part of charged as well as neutral currents should give us leading A_1 (if they exist) or B mesons, etc. For an inkling of things to come at one of the next Neutrino Conferences, I will show a graph from very recent work by Mary Gaillard and collaborators(13), whose predictions on charged-current fragmentation products are timely enough to include charmed mesons of various stripes (Fig. 33).

New-Particle Production

No self-respecting field of physics would want to be represented at this meeting without at least a hint at "New-Particle" production within its confines. W. Chen and his collaborators (Cornell - Michigan State) at FNAL fill this void for the charged-lepton scattering field by first news of the observation of 2- and 3- muon events in muon interactions at 150 GeV.(14)

FNAL Experiment 26 , designed for final-state muon recognition in deeply inelastic scattering out to very small cross-sections, clearly is a sensitive instrument for the recognition of several final-state muons emitted into its phase space acceptance. By virtue of its single-purpose concept, it is, however, not informative beyond charge and momentum of final-state muons. Fig. 34 gives examples of the reconstructed tracks, Fig. 35 an intriguing hint at a threshold for dimuon events around $W \approx 6$. A follow-up experiment presently in the set-up stage will have vastly superior statistics, so that we can expect a thorough investigation of this interesting question in the near future.

Conclusion

It was my purpose in the preparation of this talk to not only give an account of what's-new-in-charged-lepton-interactions, but also to indicate to an audience knowledgeable of neutral lepton interactions the close similarities in the phenomenological aspects of final state descriptions of the two fields. Notwithstanding the great discrepancy in interaction strengths due to W or virtual photon exchange, which at this time manifests itself mainly in the vastly different amounts of data to be interpreted, the fact that we are dealing with two local probes of the same hadronic currents makes for fruitful comparison where neutrino data exist. The richer structure of the weak current should make us expect a great deal of exciting data as the hadronic final state picture unfolds from the new neutrino experiments.

Acknowledgments

I would like to thank the organizers of the International Neutrino Conference, and particularly Professor Helmut Faissner, for their hospitality during the Conference. The readiness of my colleagues from the SLAC/MIT and Chicago/Harvard/Illinois/Oxford Collaborations to make much unpublished material available to me is gratefully acknowledged.

References

1) The neutrino comparisons are from:
J.W. Chapman et al., Phys. Rev. D14, 14 (1976);
B. Roe, Proc. of the 1975 Int. Symposium on Lepton and Photon Interactions at High Energies, Stanford (1975);
and private communications from Drs. A. Seidl, J. Van der Velde, and Malcolm Derrick.

2) C. del Papa et al., (Santa Cruz-SLAC Collaboration) UCSC Preprint 76-052, (to be published in Phys. Rev. D).

3) C. del Papa et al., Phys. Rev. D13, 2934 (1976).

4) R. Schwitters, Proc. of the 1975 Int. Symposium on Lepton and Photon Interactions at High Energies, Stanford (1975).

5) R. Feynman, Photon-Hadron Interactions, Benjamin Publishers, New York (1972).

6) See, e.g., the pp data at 100 and 400 GeV/c of C. Bromberg et al; University of Rochester preprint COO-3065-138 (1976); to be published in Nucl. Phys. B.

7) G. Chu and J.F. Gunion, Phys. Rev. D10, 3672 (1974).

8) J.T. Dakin, and G.J. Feldman, Phys. Rev. D8, 2862 (1973).

9) J. Kuti and V.F. Weisskopf, Phys. Rev. D4, 3418 (1971);
R. McElhaney and S.F. Tuan, Phys. Rev. D8, 2267 (1973).

10) C.A. Heusch, Proc. of the Int. Conf. on High Energy Physics, Palermo, Italy (1975).

11) See, e.g., G. Wolf, Proc. of the Int. Symposium on Lepton and Photon Interactions at High Energies, Stanford (1975).

12) K.Berkelman, Proc. of the Int. Symposium on Electron and Photon Interactions at High Energies, Cornell University (1971).

13) M.K. Gaillard, S.A. Jackson, and D.V. Nanopoulos, Nucl Phys. B102, 326 (1976).

14) K.W. Chen, Michigan State preprint MSU-CSL-33 (1976).

Figure Captions

1) Schematic view of SLAC Experiment 97 (SLAC-MIT Collaboration), using 20.5 GeV electron beam.

2) Schematic top view of SLAC Experiments 72, 104 (UC Santa Cruz-SLAC Collaboration), using 14 GeV μ^+ beam; 3 cameras view streamer chamber through magnet yoke.

3) Schematic top view of FNAL Experiment 98 (Chicago-Harvard-Illinois-Oxford Collaboration). $S_{0,1}$ are multiwire proportional chambers, $S_{2...6}$ are multiwire spark chambers. Old Chicago cyclotron magnet is in center.

4) Mean charged hadron multiplicity from UCSC-SLAC μp experiment, vs. s, with comparison data from γp, $\pi^{\pm} p$ collisions. Neutrino curve is $\langle n \rangle \sim 1.09 + 1.13 \ln s$ fit from B. Roe, ref. (1).

5) Q^2 dependence of mean multiplicity for two energy bins, for forward emitted charged hadrons ($0.3 \leq x_F \leq 0.8$), for μp and μn collisions (UCSC-SLAC).

6) Comparison of mean charged-hadron multiplicities from μp collisions and e^+e^- annihilation. To account for difference in incoming baryon number, either subtract one-prong events from μp sample or use Q value ($= \sqrt{s} - \Sigma m_{in}$) as energy variable. Upper scale: Q value for μp collisions.

7) Mean charged-hadron multiplicities: comparison of μp and μn energy dependence (UCSC-SLAC).

8) Fractional topological cross-sections for μp, μn collisions in energy interval $2.3 \leq W \leq 4.2$ GeV. Multiplicities $n > 6$ can be neglected at these energies. Q^2 ranges from 0.3 to 1.0 (UCSC-SLAC).

9) Q^2 dependence of fractional topological cross-sections for μp, μn collisions for energy bin $2.8 \leq W \leq 3.6$. Full points at $Q^2 = 0$ indicate photoproduction values, drawn across graphs for comparison purposes.

10) Energy dependence of fractional cross-sections $\alpha_n = \sigma_{n,\mathrm{direct}}/\sigma_{n,\mathrm{direct + exchange}}$. Preliminary data from UCSC-SLAC experiment.

11) Q^2 dependence of fractional direct cross-sections α_n from preliminary analysis of UCSC-SLAC data. At $Q^2 = 0$, photoproduction comparison values are extracted from data in E. Kogan's thesis, Weizmann Institute of Science (1975), (unpublished).

12) Interaction structure functions $F_{\mu p}$ for the production of (a) negative, (b) positive, (c) all charged hadrons in μp collisions. For positives, no data are given at $z = \frac{1}{\nu} E_{\mathrm{lab}}^{\mathrm{had}}$ values below 0.4 due to π^+/p ambiguities in streamer chamber analysis (UCSC-SLAC). e^+e^- comparison from Ref. 4.

13) Interaction structure function $F_{\mu n}$ in terms of fractional longitudinal momentum $x' \simeq x_F$, for $s > 100$ (FNAL). e^+e^- comparison from Ref. 4.

14) Comparison of quark fragmentation functions extracted from μp experiment with neutrino data. Eye-fit curves indicate agreement between comparable quantities.

15) Transverse momentum structure function for μN collisions from FNAL experiment ($s > 100$), for three x_F ranges: curve C indicates diffractive forward component.

16) a: Mean transverse momentum dependence on fractional longitudinal momentum x_F, for various Q^2 ranges, from μp collisions (UCSC-SLAC). Cutoff at $x_F = -0.3$ due to streamer-chamber inefficiency.

b: For comparison, x_F dependence of negative hadrons from high-energy pp collisions (FNAL-Michigan Collaboration).

17) Transverse momentum dependence of hadrons emitted from μp collisions, for two x_F intervals. Single and double exponential fits as discussed in text (UCSC-SLAC).

18) Energy dependence of mean transverse momentum for various x_F bins. Φ points with eye-fit curves are neutrino comparisons from FNAL-Michigan Collaboration. (UCSC-SLAC).

19) Mean transverse momentum for forward-emitted hadrons from high-energy μp collisions, vs. Q^2(SLAC-MIT). Dashed curve indicates trend of neutrino data from FNAL-Michigan Collaboration.

20) Charge ratio for forward-emitted ($0.4 < x_F < 0.85$) hadrons (full points) and pions (open points), vs. Q^2. ρ^0 contribution has been subtracted out. Neutron data result from deuteron-proton subtraction. (SLAC-MIT)

21) Charge ratio for forward-emitted pions only, as a function of electron scattering scaling variable x. Cuts as in previous figure. (SLAC-MIT)

22) Particle ratios for forward-emitted hadrons in ep scattering, with photoproduction comparison point. ρ^0 contribution has been subtracted out (SLAC-MIT).

23) Dipion invariant mass plot from 4C fit sample of UCSC-SLAC $\mu p \to \mu p \pi^+ \pi^-$ candidates, for three Q^2 bins and $W > 2$.

24) Dipion mass plots from forward-emitted hadrons in FNAL experiment, for four Q^2 bins, at high energies.

25) Coherent ρ^0 production at FNAL: preliminary evidence of coherent forward peak in carbon, $\sim e^{38t}$. Incoherent e^{7t} trend coincides with t dependence in μp experiment.

26) Cross-sections for ρ^0 (Φ) and ω^0 ($\ast$) production by μp collisions in UCSC-SLAC streamer chamber experiment, vs. Q^2.

27) Total ρ^0 photoproduction cross-section: open points were determined from extrapolation to $Q^2 = 0$ of FNAL muon scattering data. Curve represents quark-model expectation on the basis of elastic πp scattering data.

28) Q^2 dependence of ρ^o electroproduction data normalized, for each W, to photoproduction values. Q^2 dependence of transverse ρ^o production as shown here, should vary approximately as $(1 + \frac{Q^2}{m_\rho^2})^{-2}$, as indicated by curve, according to the vector dominance model. (SLAC-MIT)

29) Fractional cross-sections for ρ^o (SLAC-MIT and UCSC-SLAC) and for ω^o (UCSC-SLAC), as a function of Q^2. All $W > 2$ for UCSC-SLAC, $W > 4$ for SLAC-MIT. Comparison values from photoproduction should have large error bars for W dependence and discrepancies between experiments.

30) Q^2 dependence of slope parameter $b(Q^2)$ from exponential fits to forward ρ^o production. Data from UCSC-SLAC ($W > 2$), SLAC-MIT ($W > 4$), and FNAL ($W > 100$).

31) Invariant-mass plot from streamer chamber events giving 1-C fits to hypothesis $\mu^+ p \rightarrow \mu^+ p \pi^+ \pi^- \pi^o$. Kinematical range: $W > 2$, $0.3 \leq Q^2 \leq 1$. (UCSC-SLAC).

32) Relative weight of ρ^o and ω^o production, as a function of Q^2, from UCSC-SLAC experiment ($2 \leq W \leq 4$ GeV). : comparison point in photoproduction.

33) Prediction by Gaillard et al., for incoherent elastic fragmentation of $W^{\pm}$ into various mesons, as a function of neutrino energy. (For model, see Ref. 13.)

34) Candidate events for $\mu^+ N \rightarrow \mu^+ \mu^- + \ldots$, $\mu^+ N \rightarrow \mu^+ \mu^- \mu^- + \ldots$ from thick-target experiment 26 (Cornell-Michigan State) at FNAL. Track chambers in back are interleaved with magnetized iron units.

35) Threshold effect of dimuon candidate appearance in excess of what can be accounted for by hadron decays etc.; from FNAL Exp. 26.

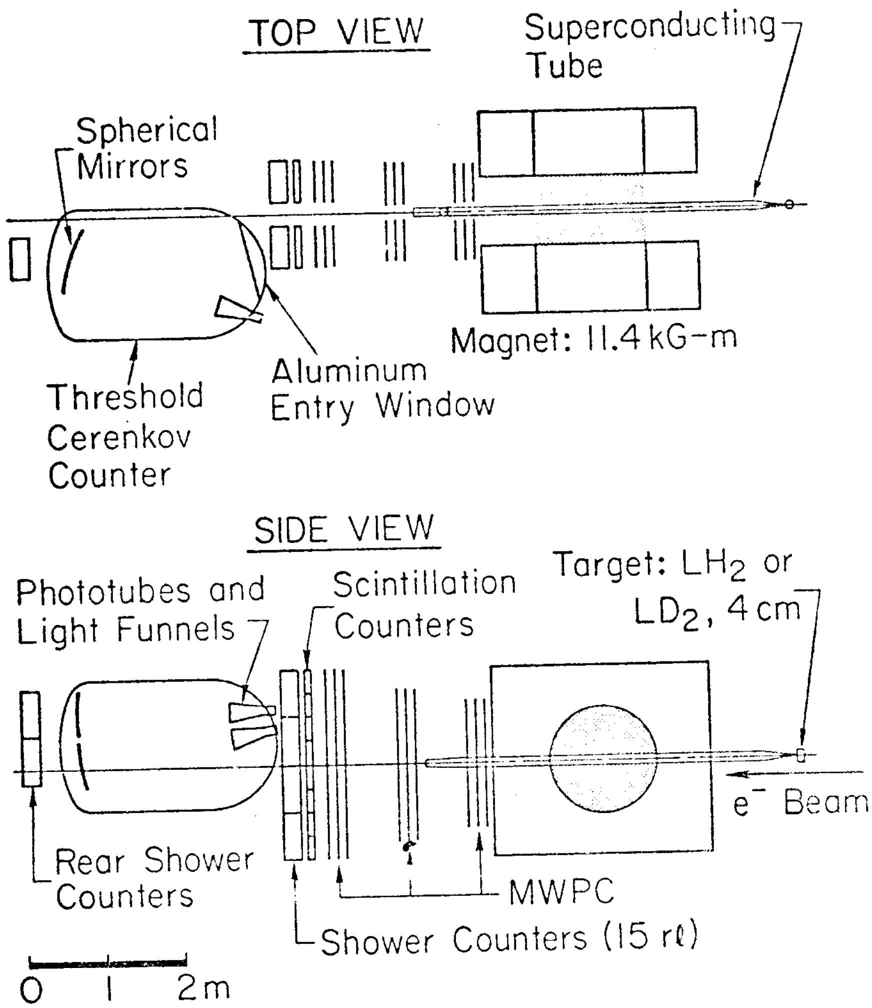

Figure 1

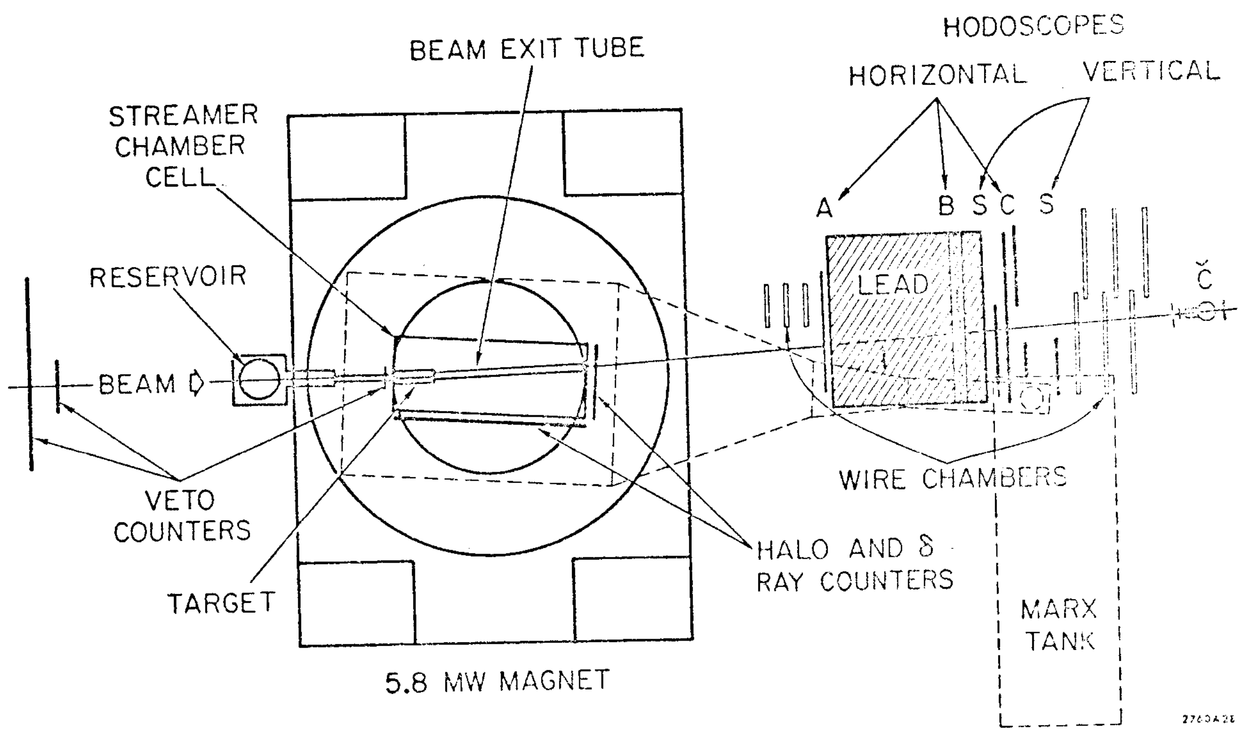

Figure 2

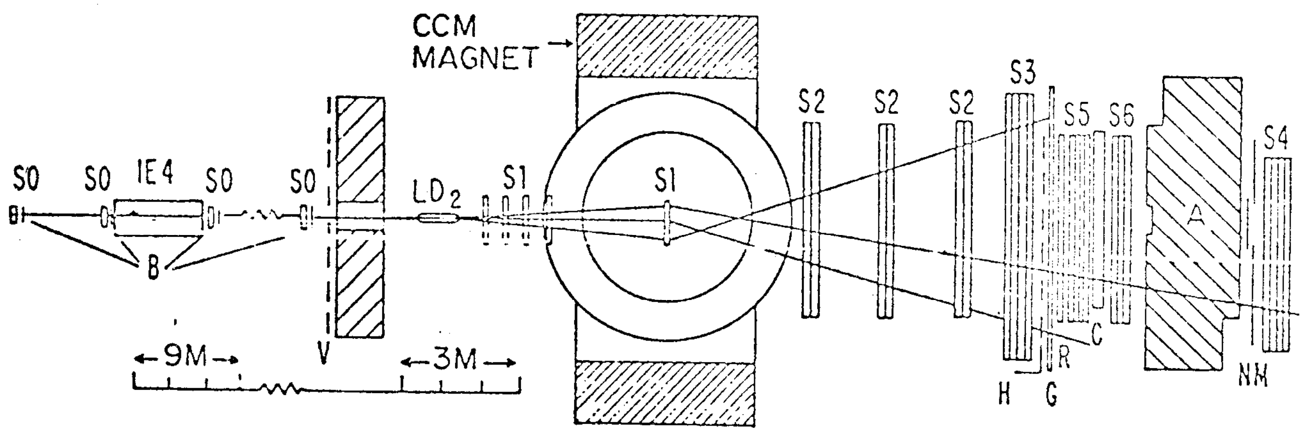

Figure 3

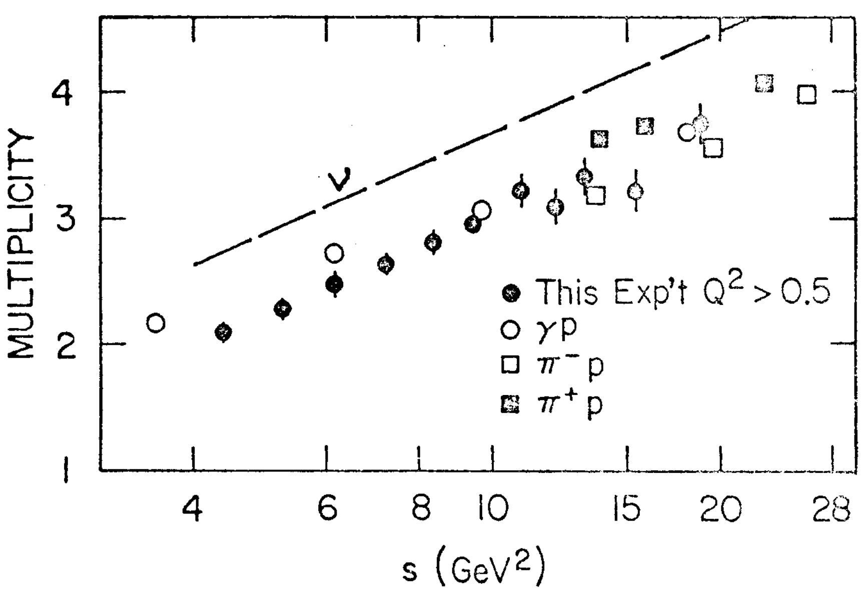

Figure 4

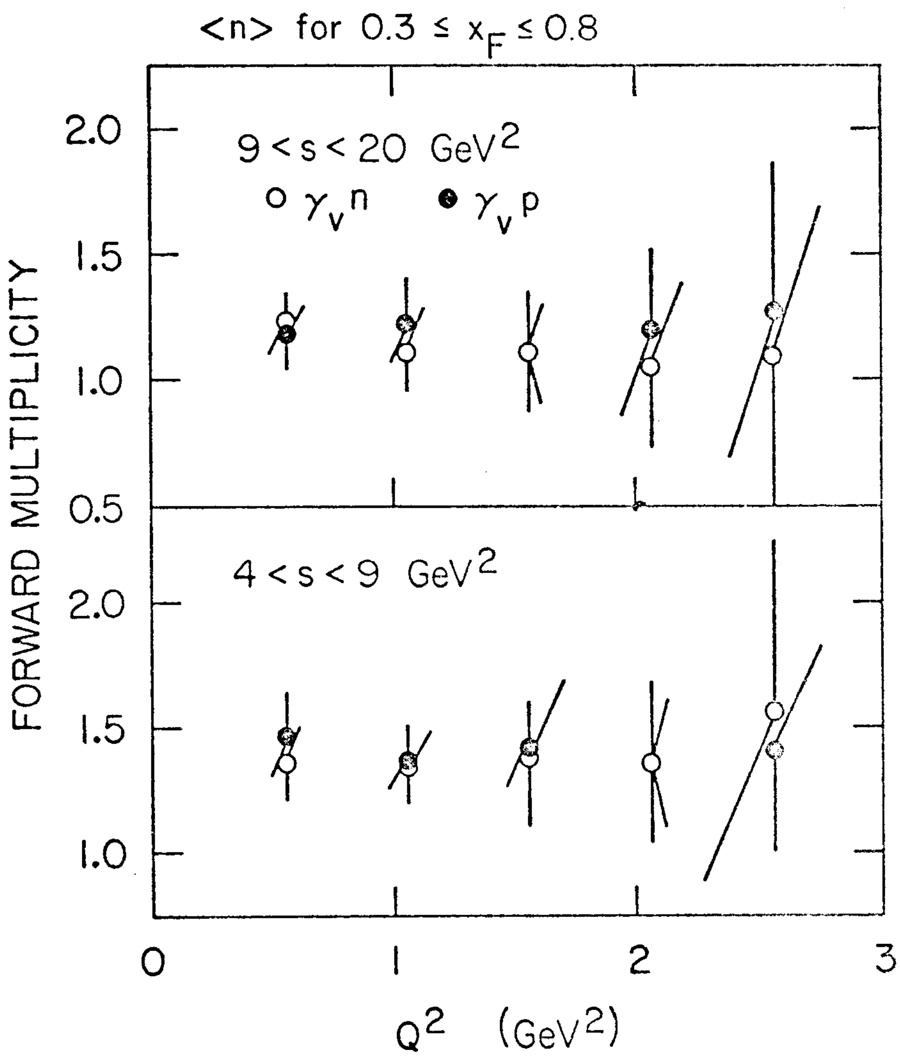

Figure 5

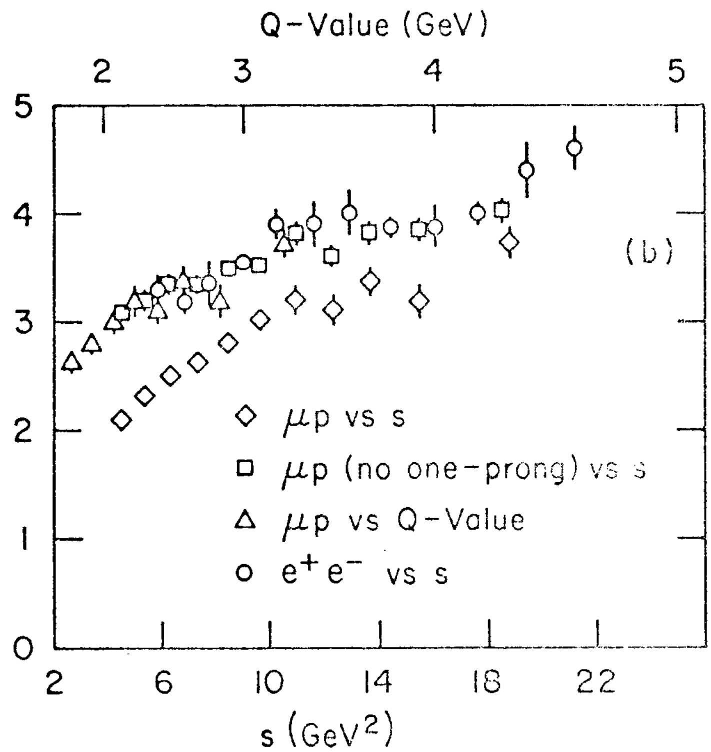

Figure 6

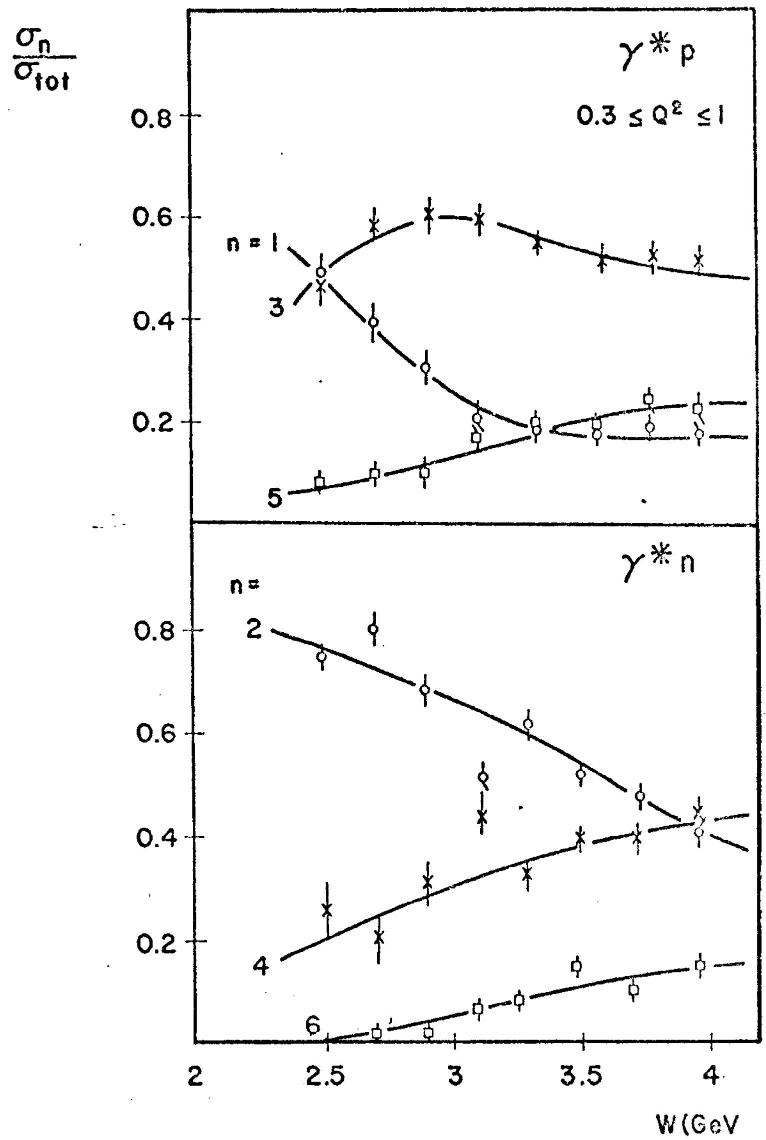

Figure 7

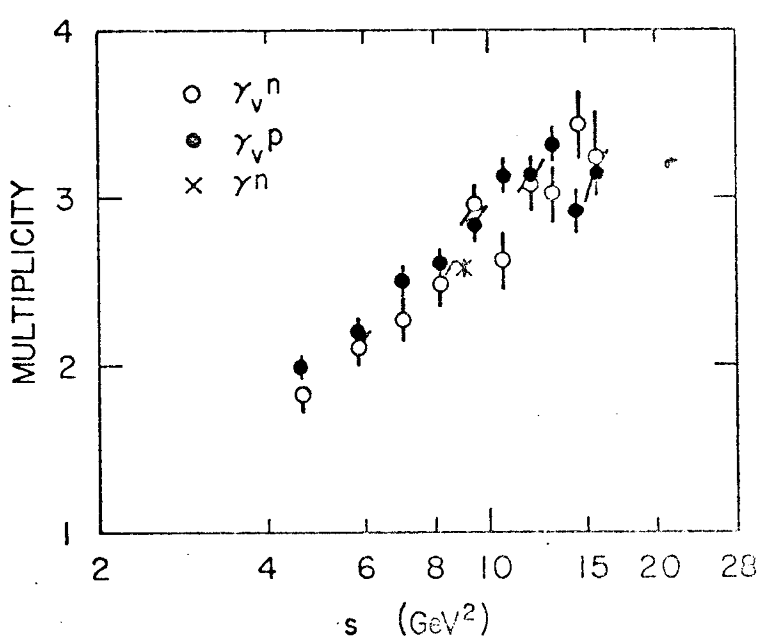

Figure 8

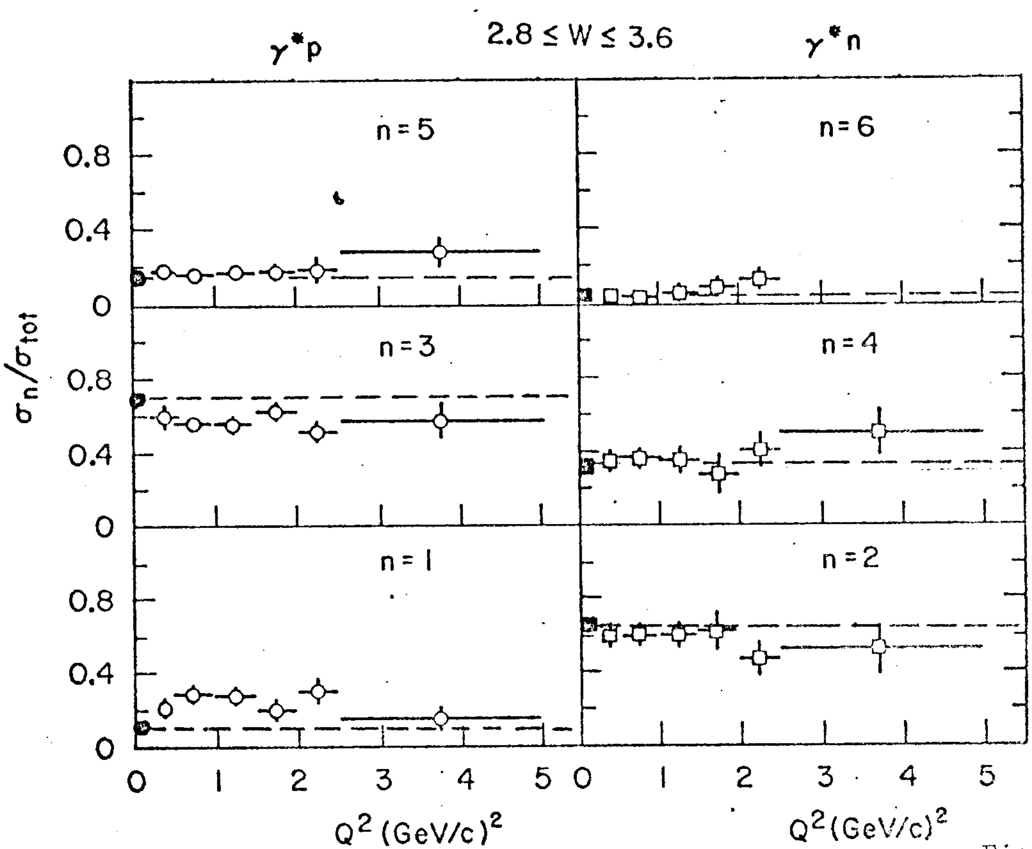

Figure 9

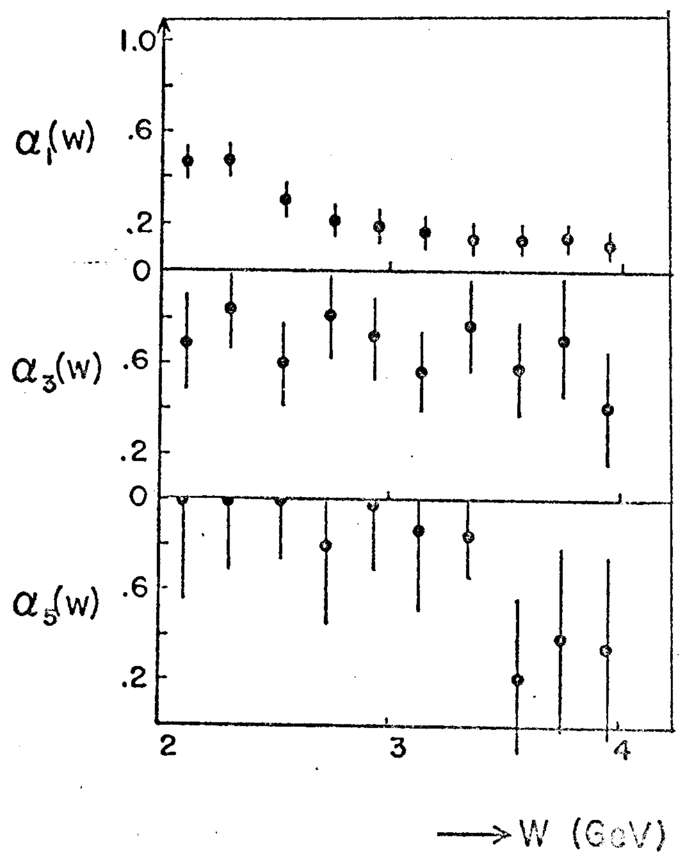

Figure 10

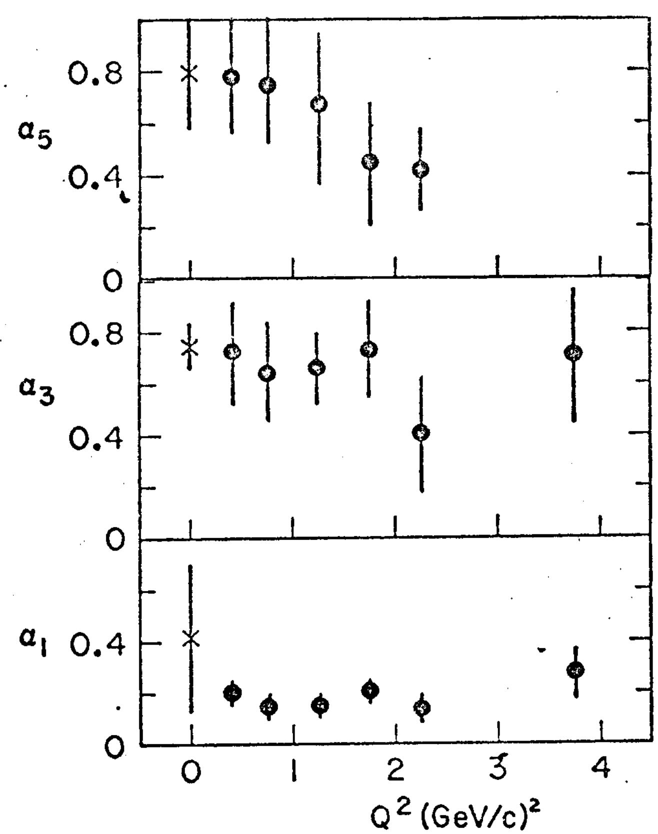

Figure 11

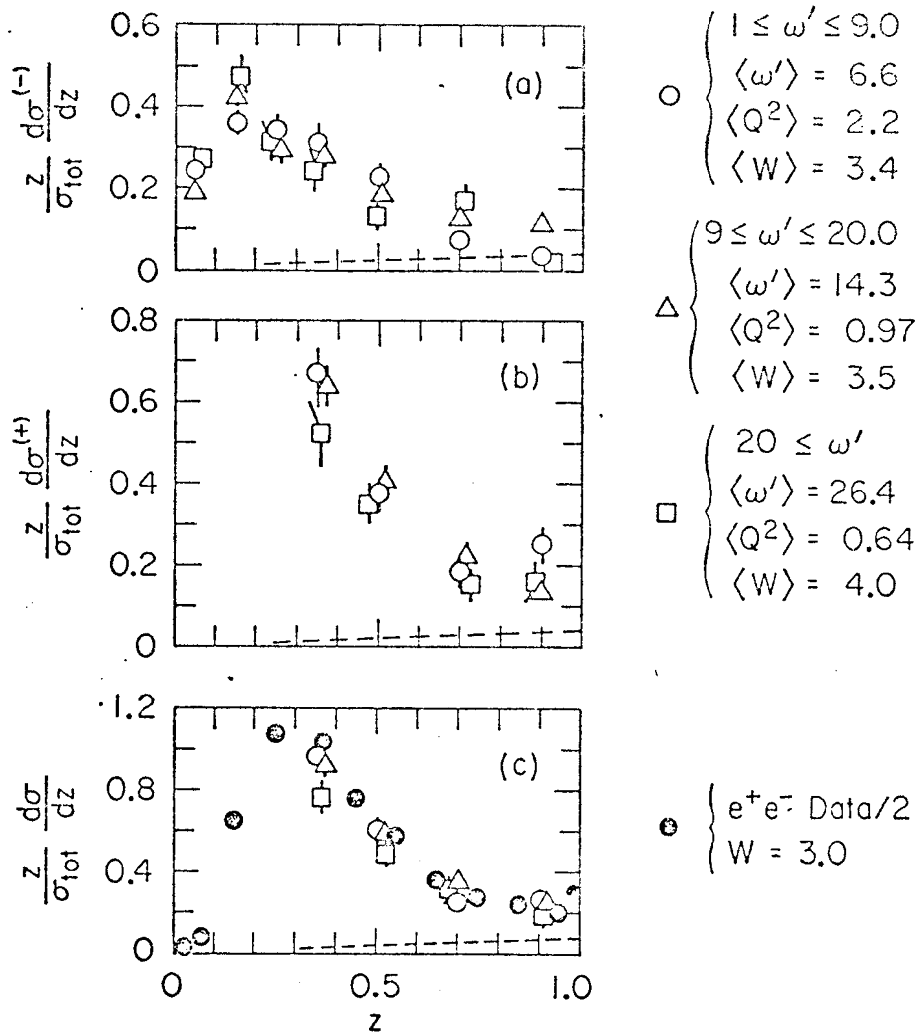

Figure 12

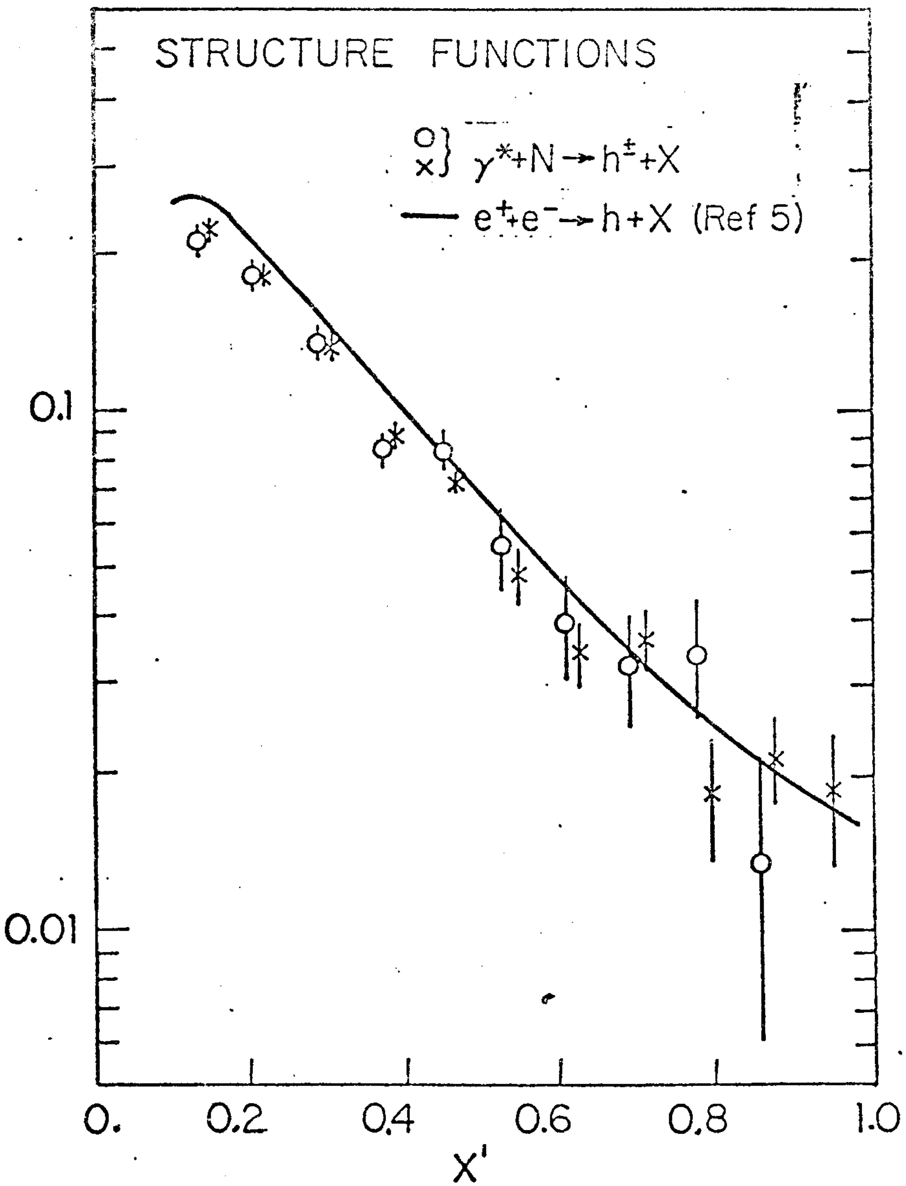

Figure 13

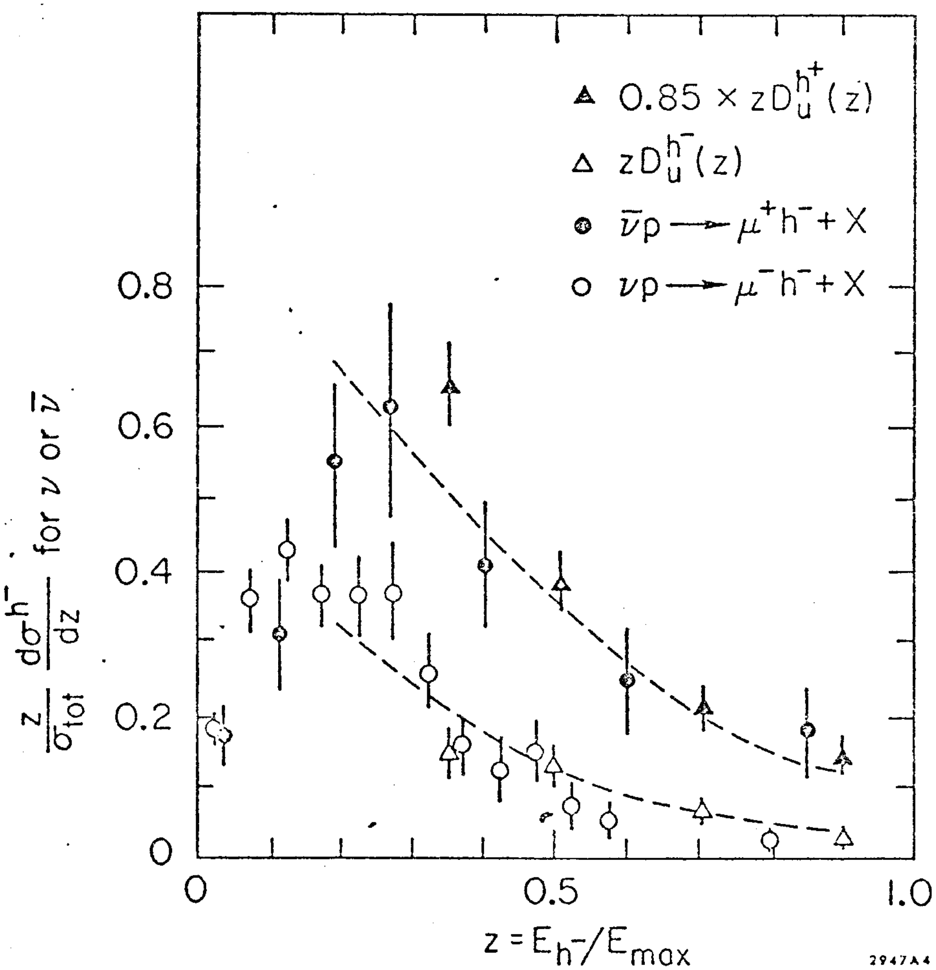

Figure 14

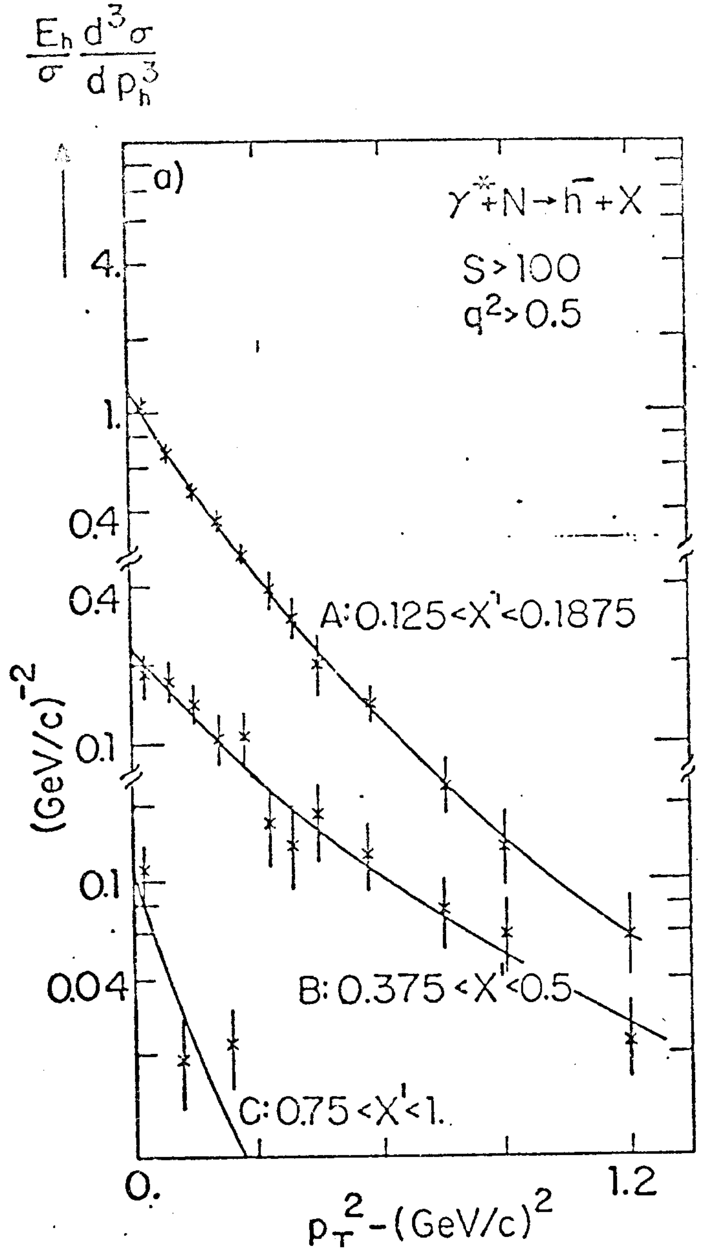

Figure 15

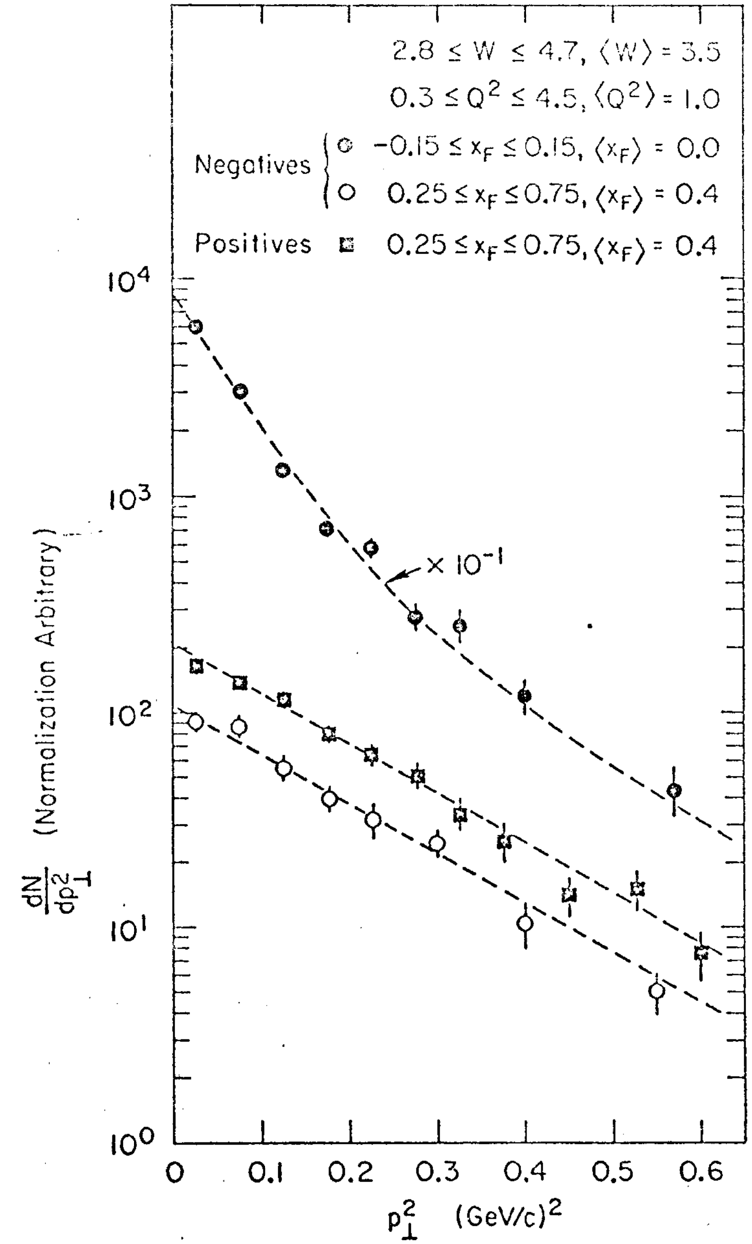

Figure 17

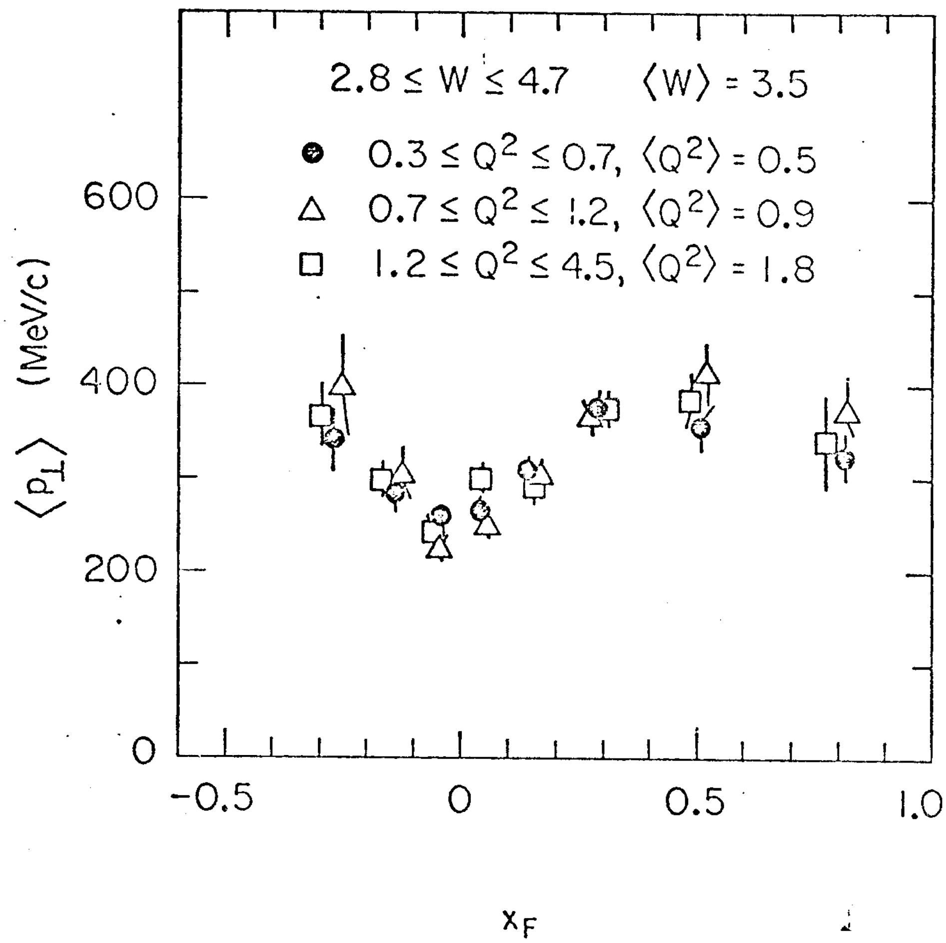

Figure 16a

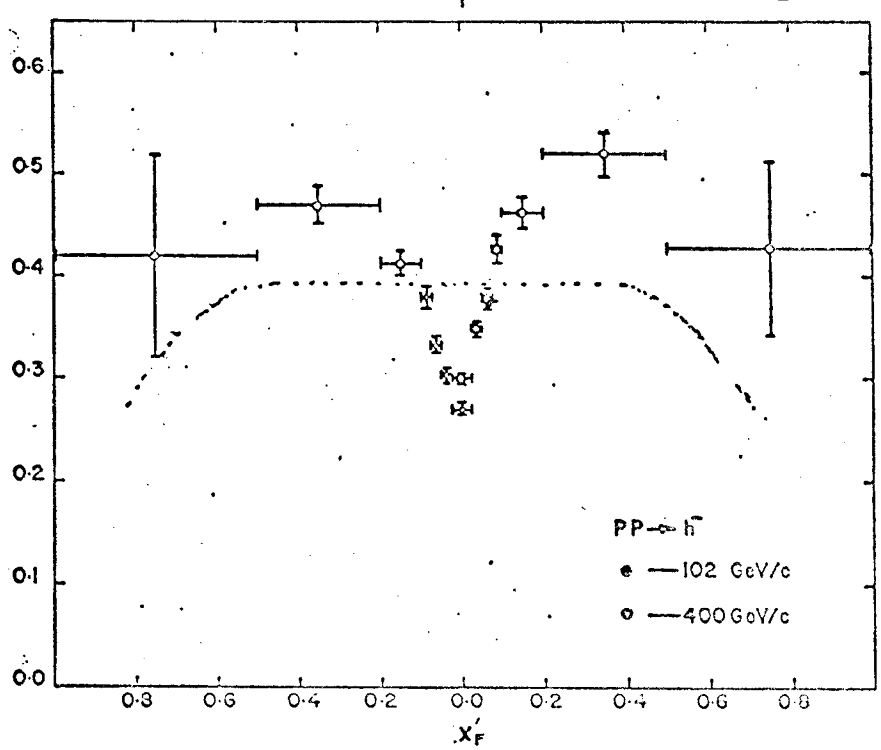

Figure 16b

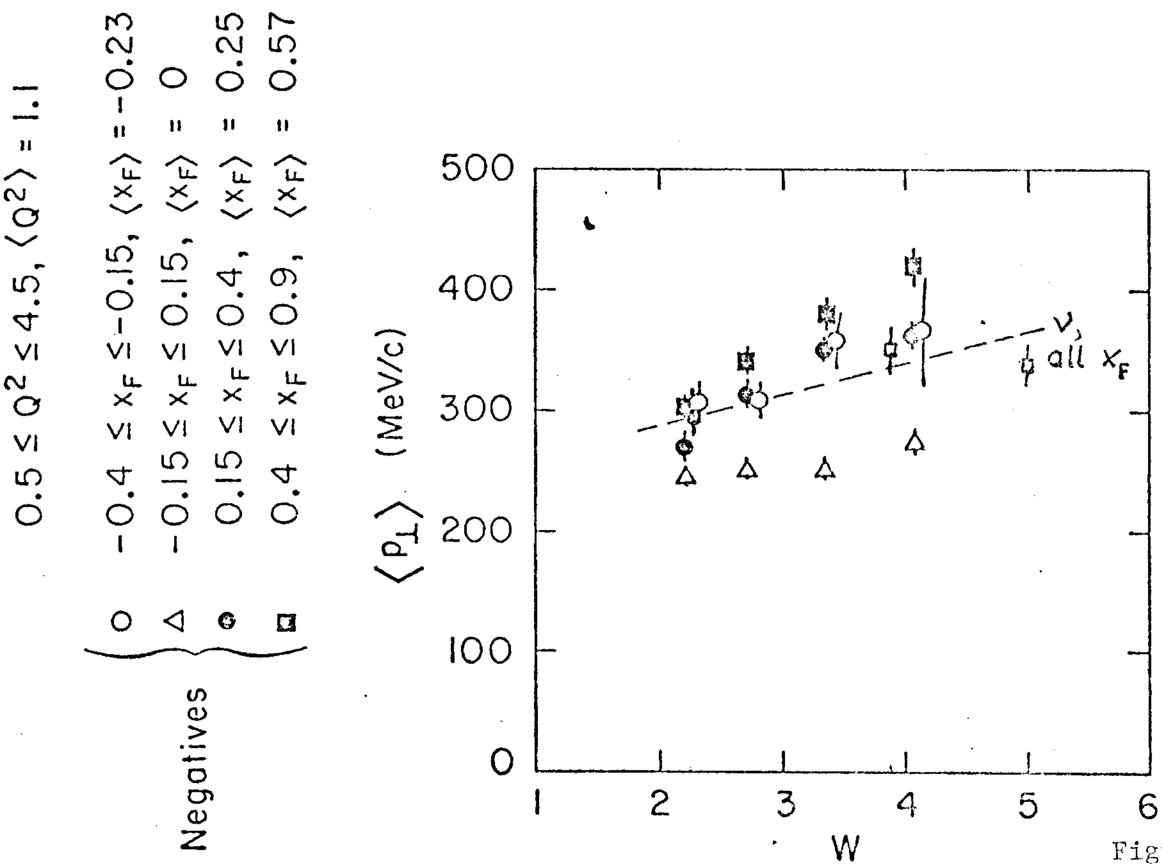
0.5 ≤ Q² ≤ 4.5, ⟨Q²⟩ = 1.1
−0.4 ≤ x_F ≤ −0.15, ⟨x_F⟩ = −0.23
−0.15 ≤ x_F ≤ 0.15, ⟨x_F⟩ = 0
0.15 ≤ x_F ≤ 0.4, ⟨x_F⟩ = 0.25
0.4 ≤ x_F ≤ 0.9, ⟨x_F⟩ = 0.57
Negatives
⟨p⊥⟩ (MeV/c)
ν, all x_F
W

Figure

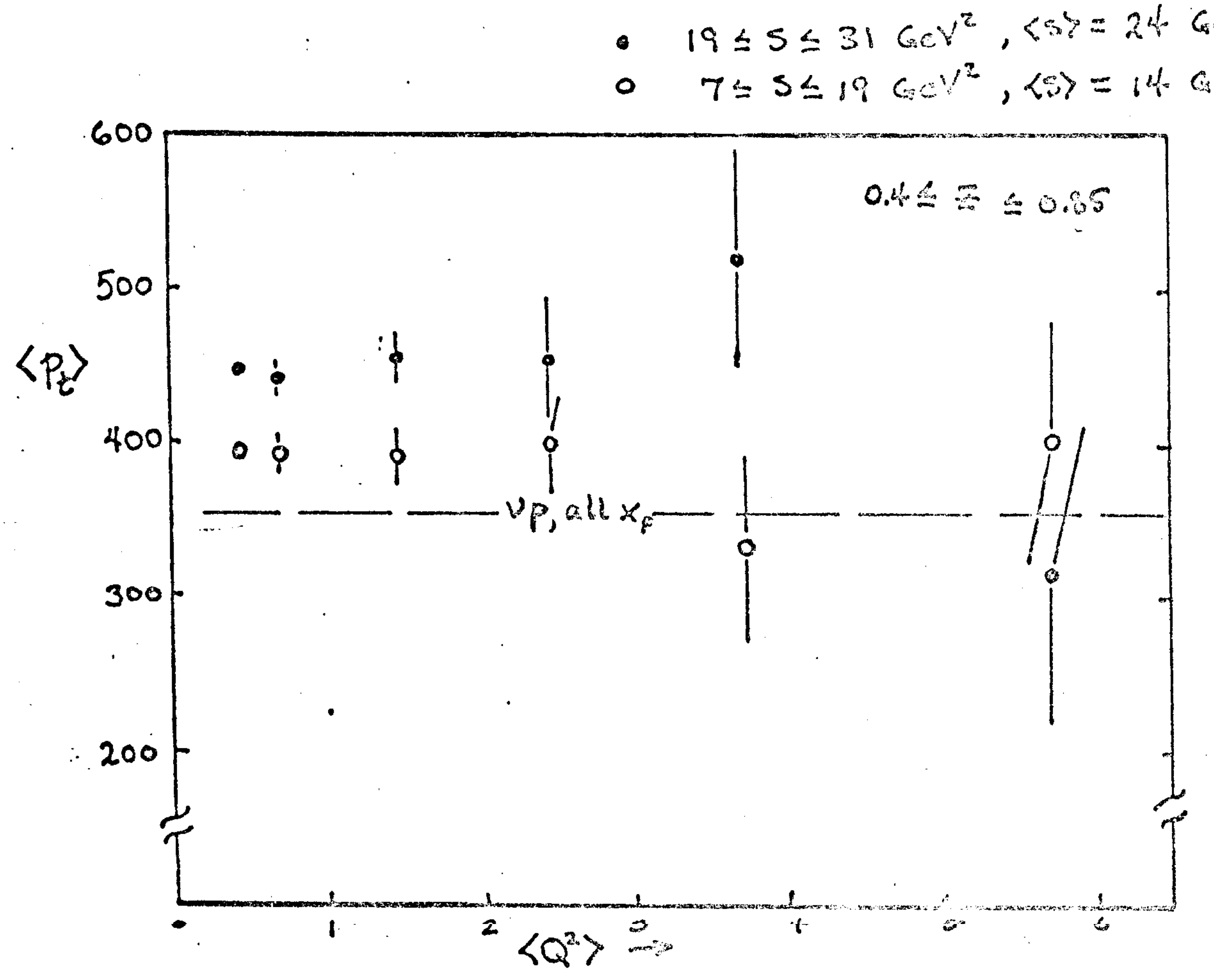
19 ≤ s ≤ 31 GeV², ⟨s⟩ = 24 G
7 ≤ s ≤ 19 GeV², ⟨s⟩ = 14 G
0.4 ≤ z ≤ 0.85
⟨p_t⟩
νp, all x_F
⟨Q²⟩

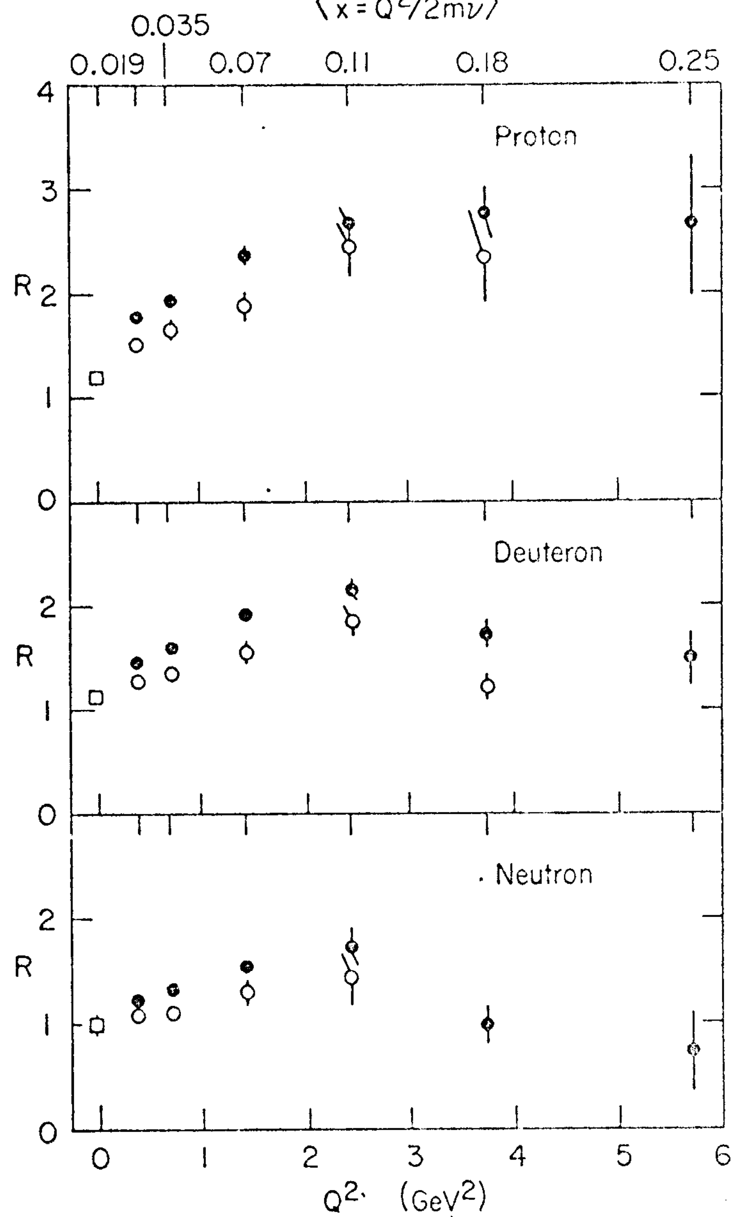

Figure 20

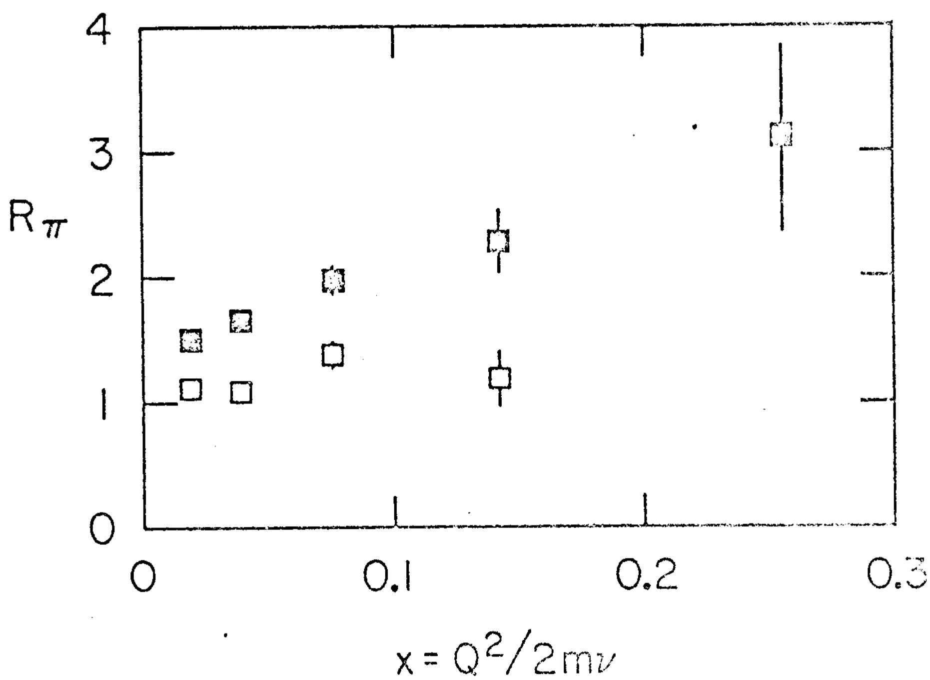

Figure 21

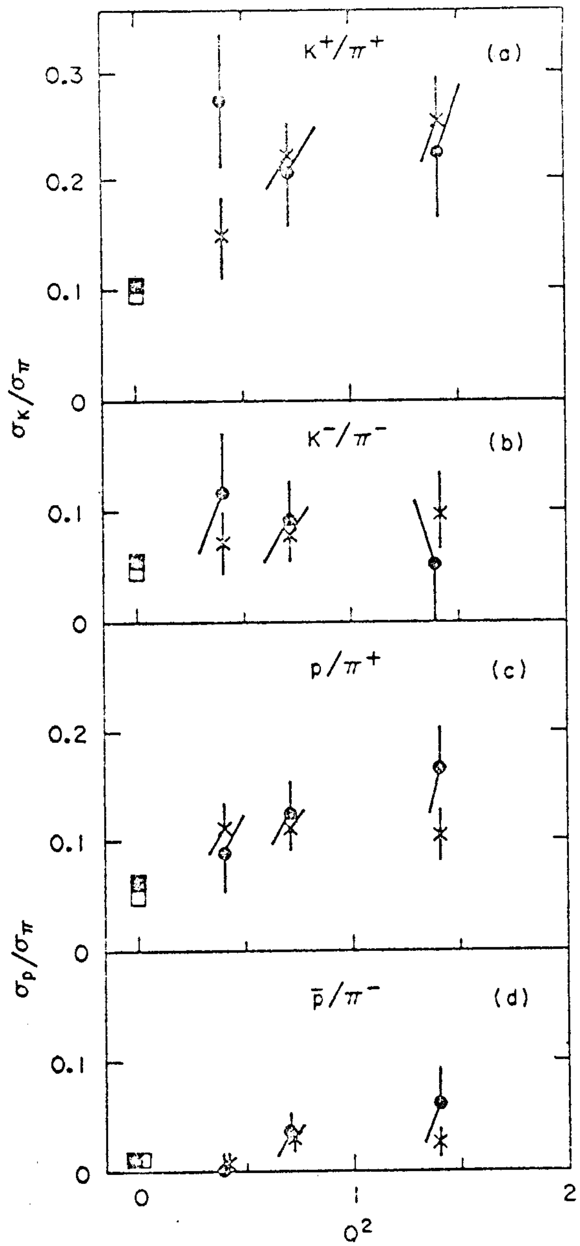

Figure 22

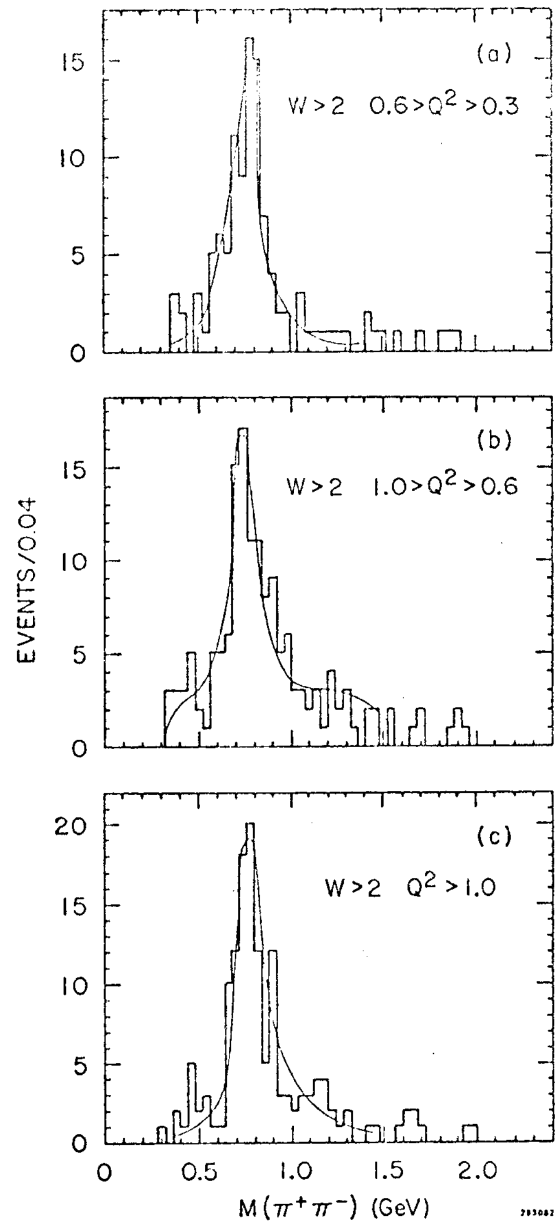

Figure 23

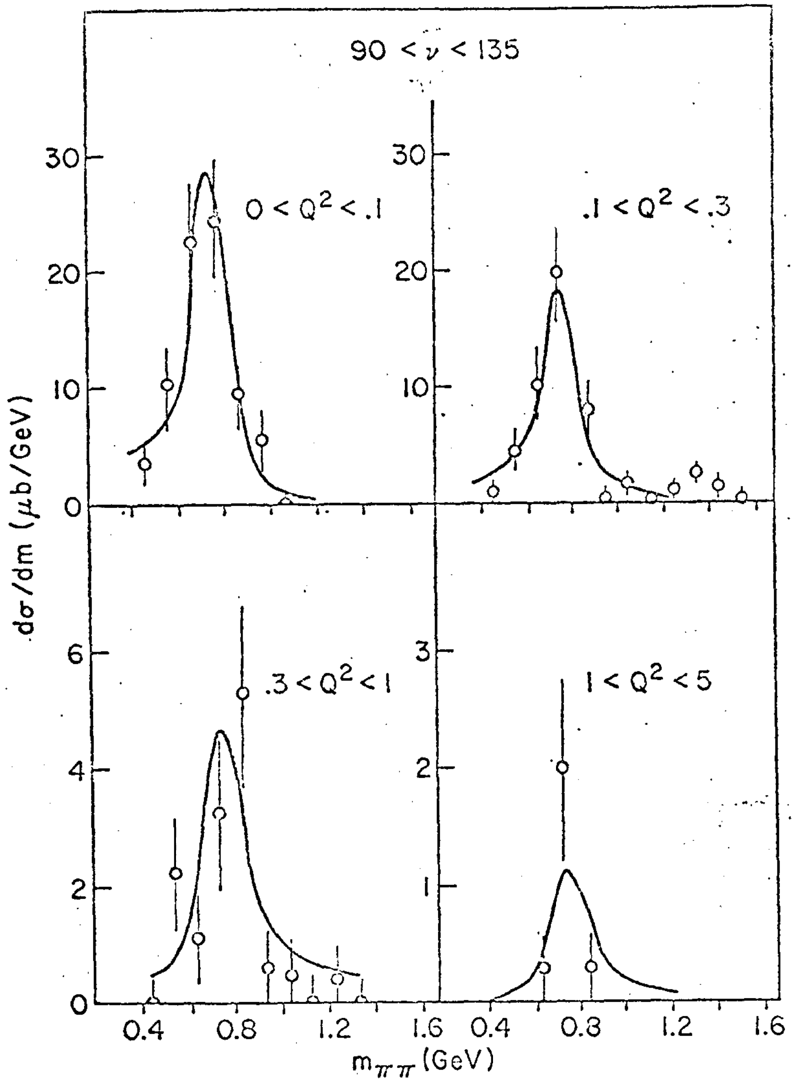

Figure 24

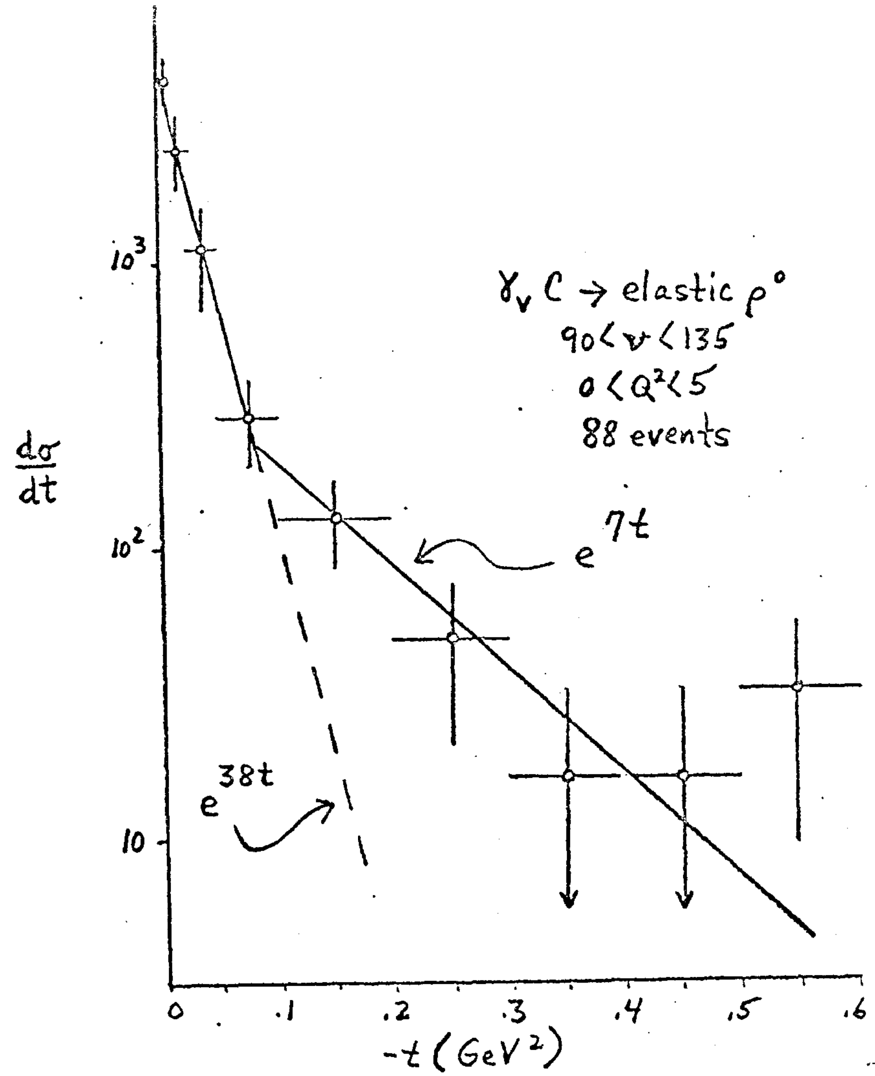

Figure 25

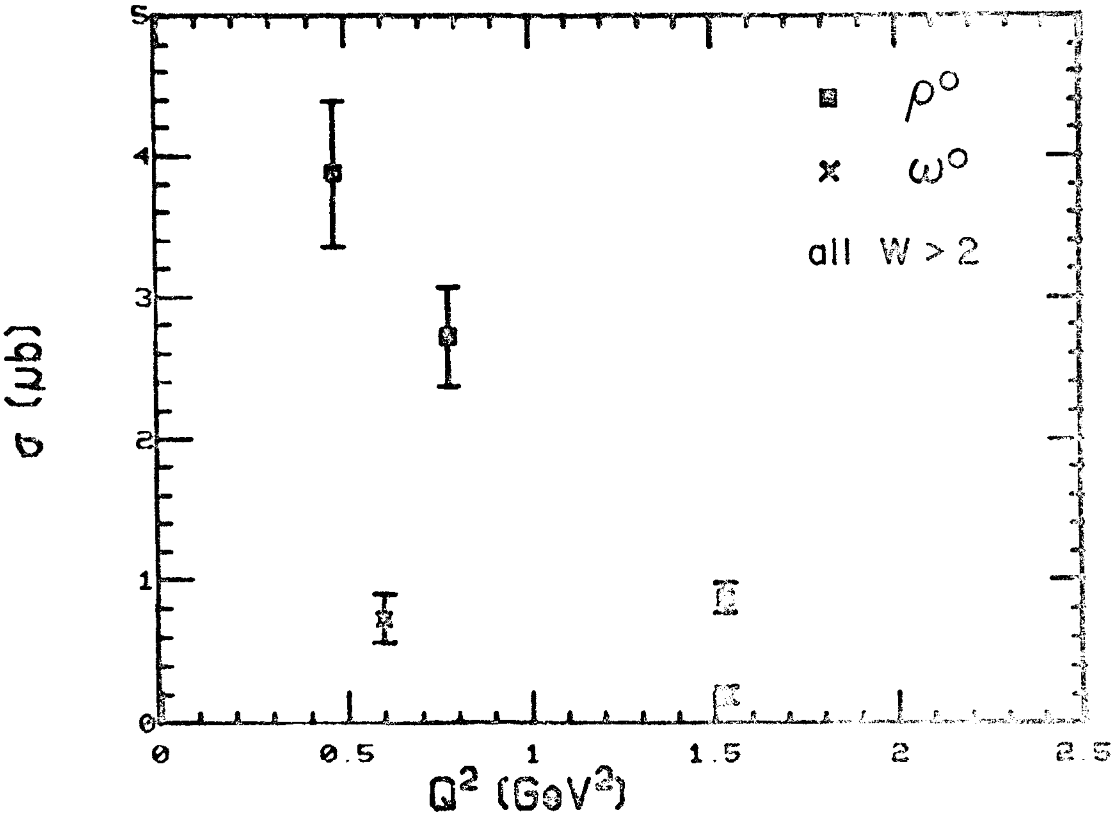

Figure 26

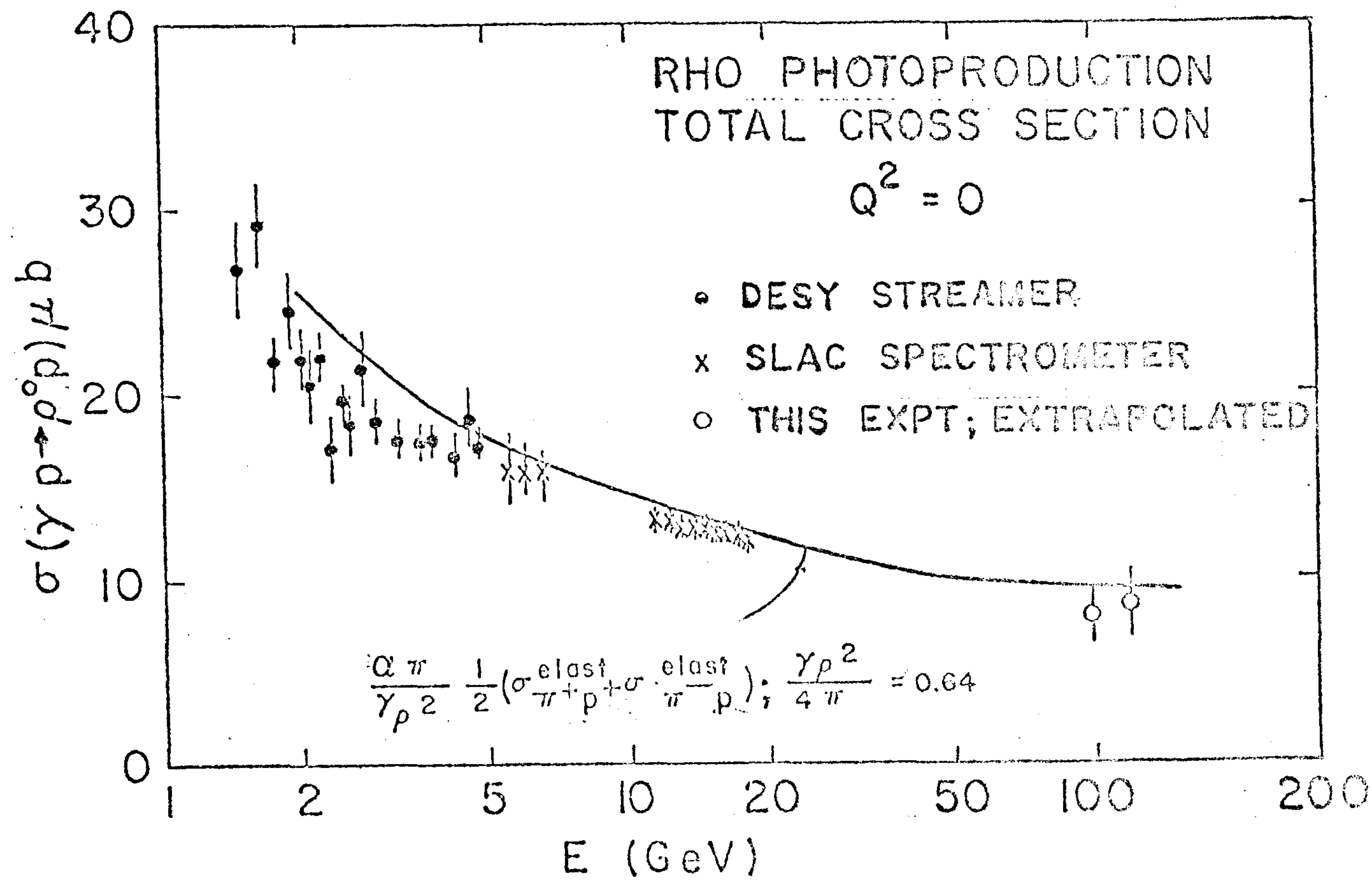

Figure 27

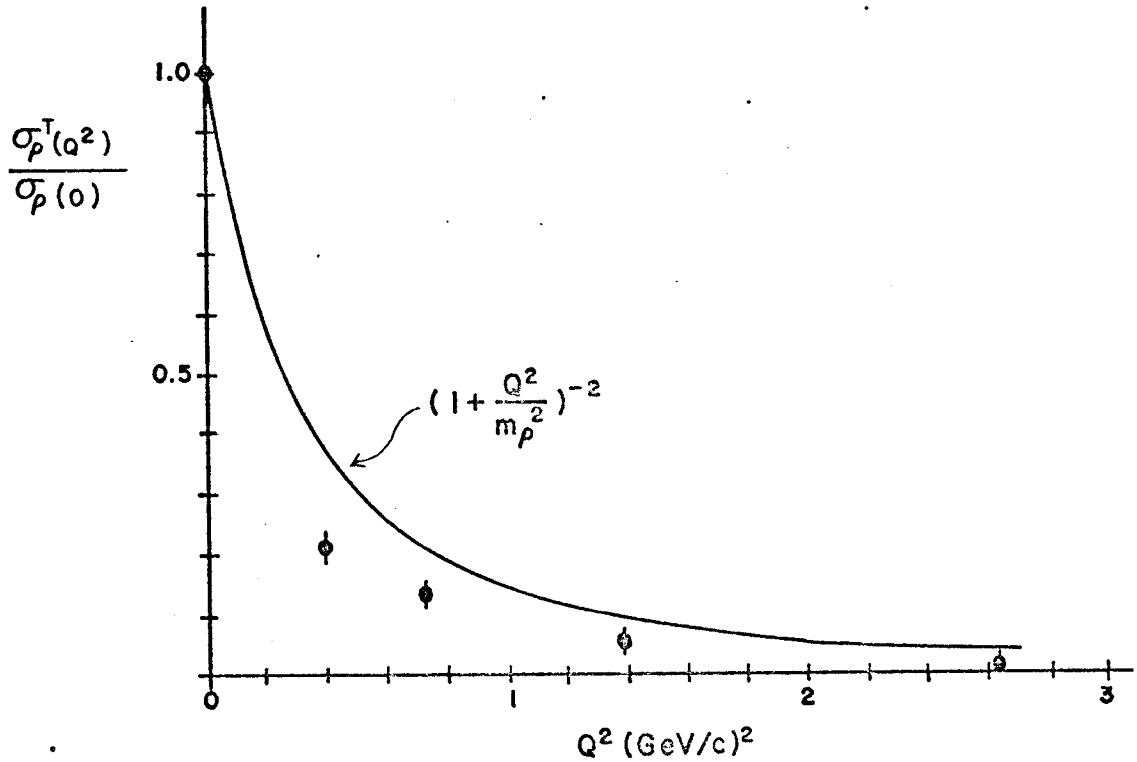

Figure 28

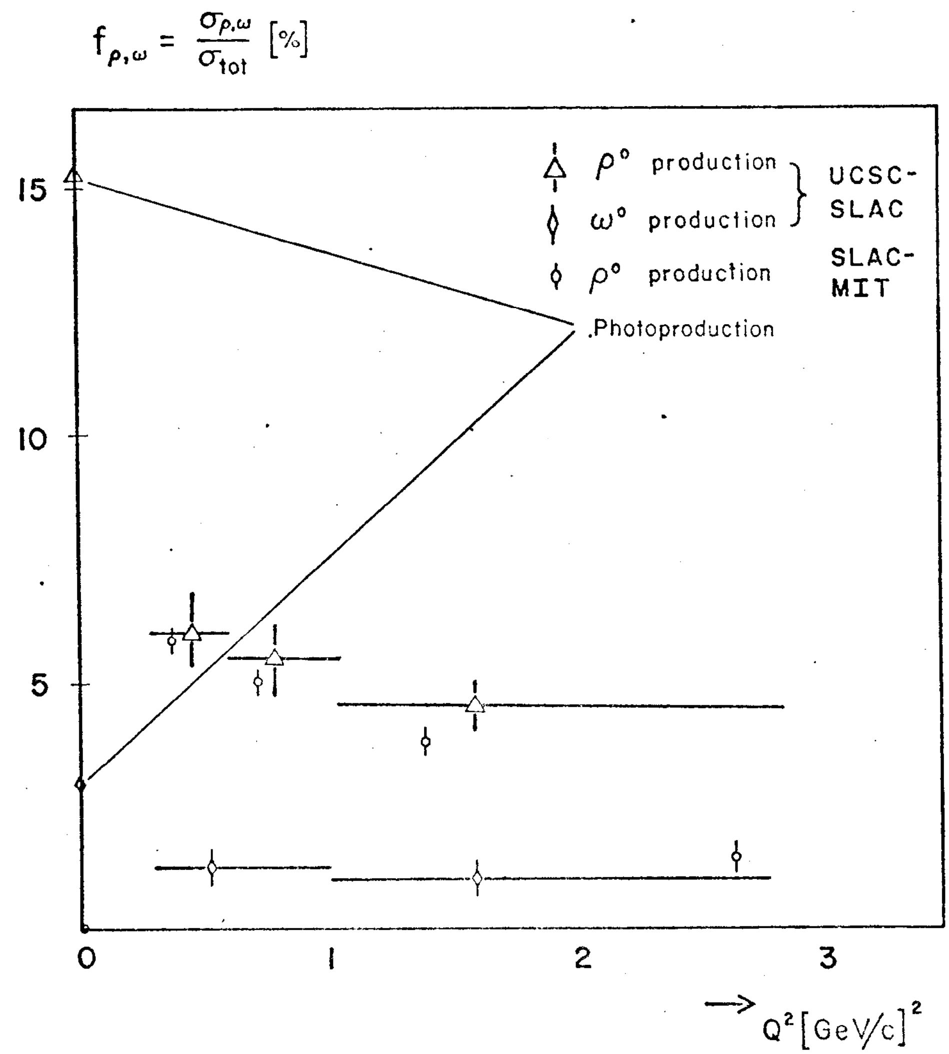

Figure 29

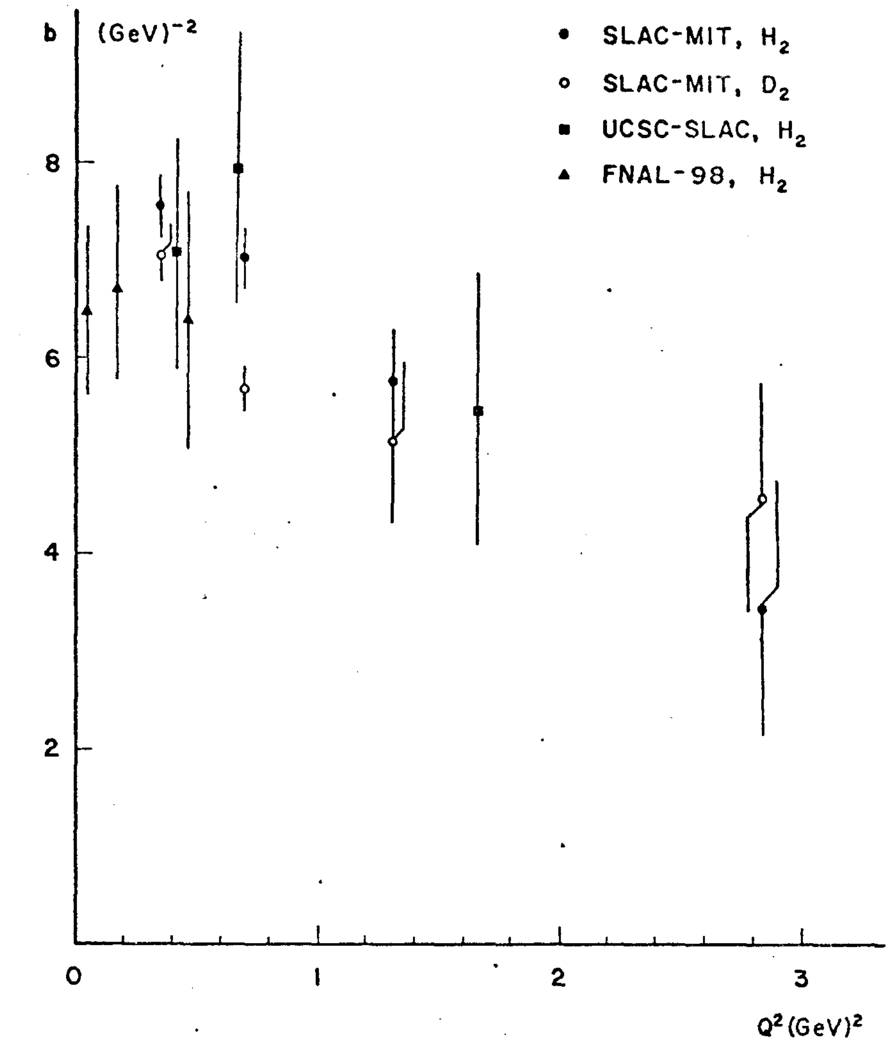

Figure 30

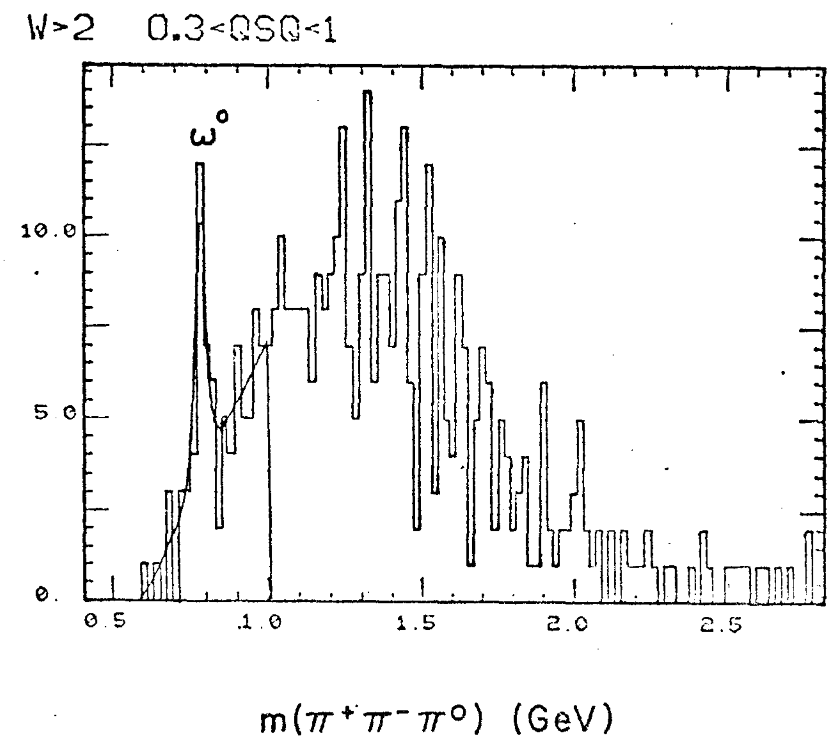

Figure 31

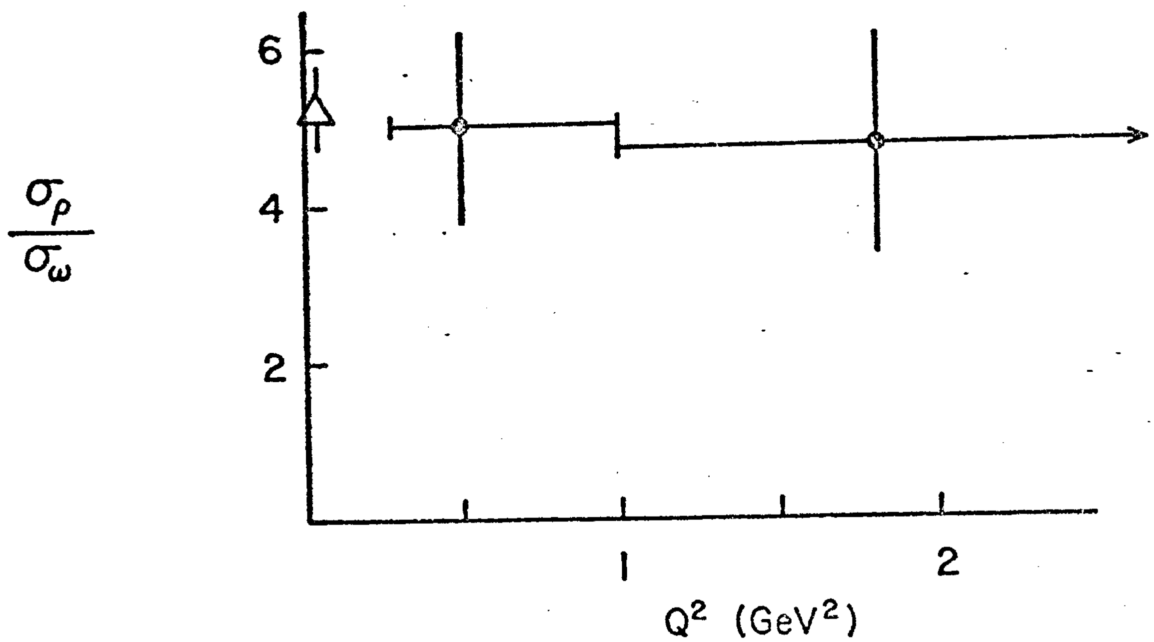

Figure 32

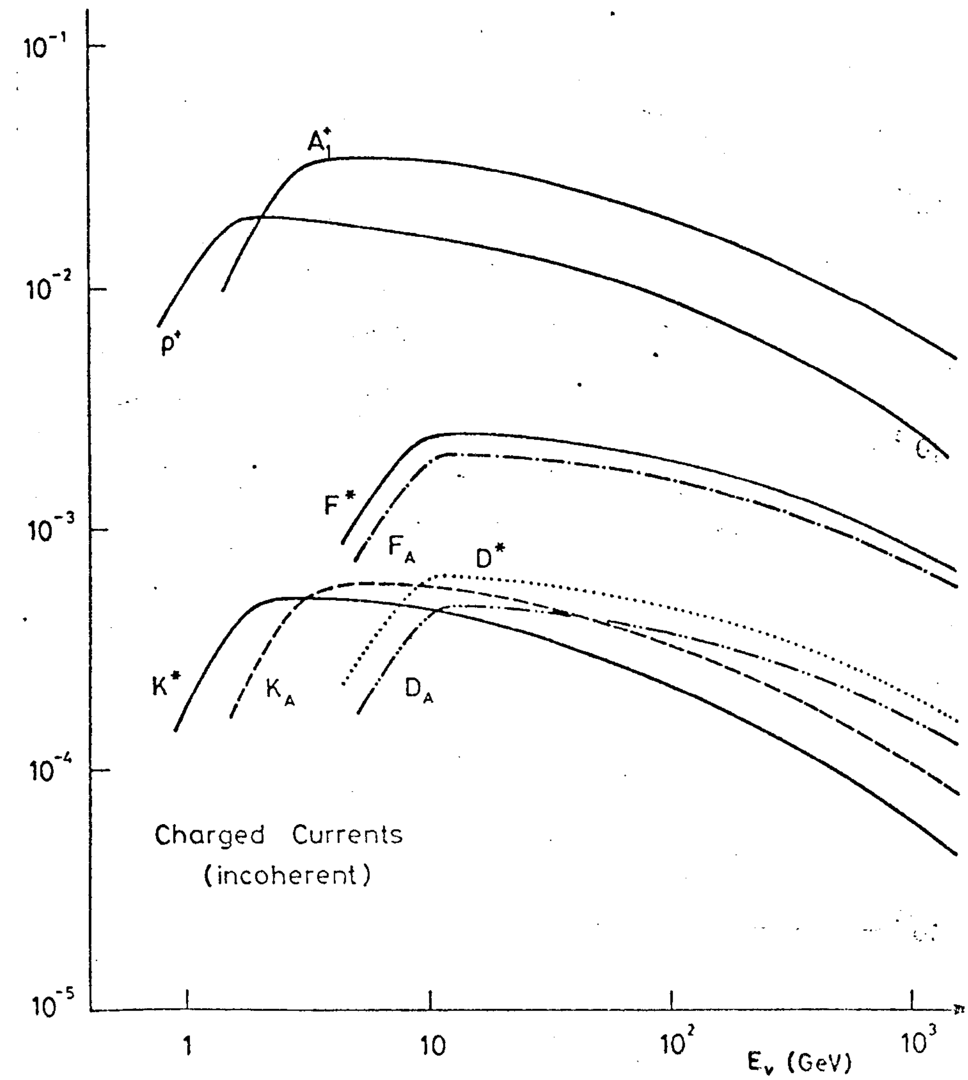

Figure 33

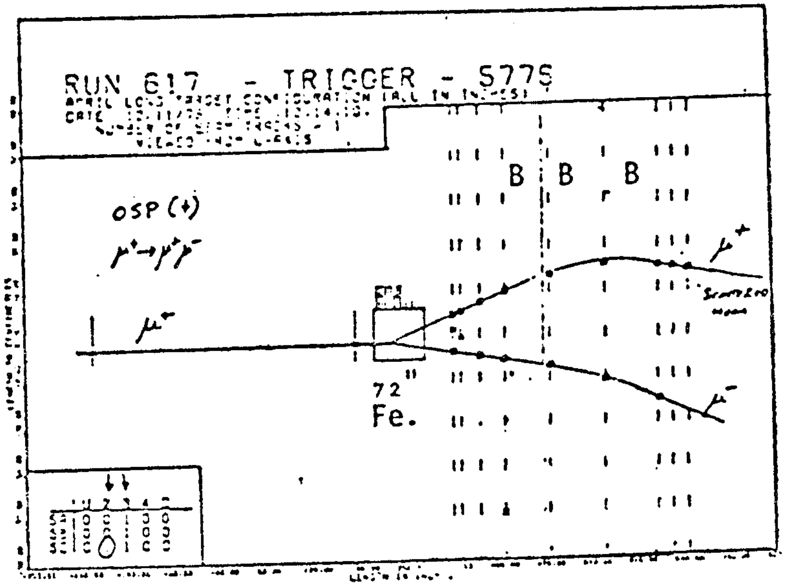

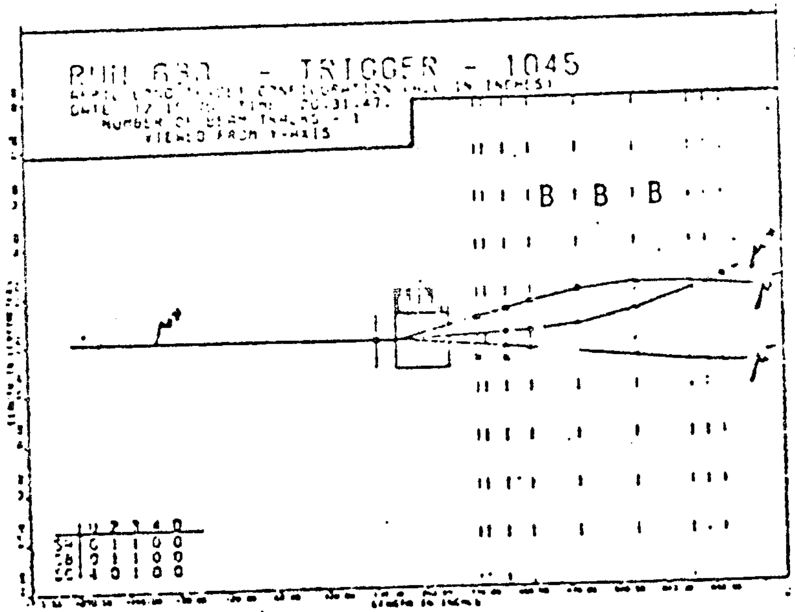

Figure 34

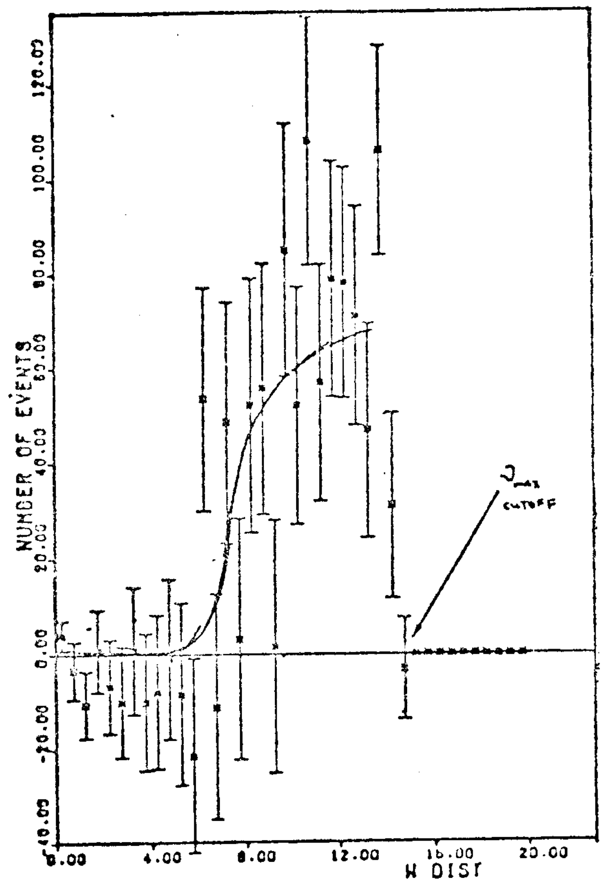

Figure 35